Available online at www.sciencedirect.com
SCIENCE DIRECT®
Journal of Computational Physics 204 (2005) 598–632
JOURNAL OF COMPUTATIONAL PHYSICS
www.elsevier.com/locate/jcp

Two-phase shock-tube problems and numerical methods of solution

C.A. Lowe *

Department of Applied Mathematics and Theoretical Physics, Centre of Mathematical Sciences, Cambridge University, Wilberforce Rd., Cambridge CB3 0WA, UK

Received 30 September 2003; received in revised form 18 October 2004; accepted 19 October 2004
Available online 23 November 2004

Abstract

The study involves the flow of compressible gas in a porous bed: We are interested in exploring the solution to a shock-tube problem that also includes a discontinuous jump in the porosity of the bed. The averaging process that is used to derive the governing system of equations introduces terms that prevent the equations taking a standard conservation form. The purpose of this work is to explore how the porosity jump effects the solution to the Riemann problem and to assess whether standard conservative and nonconservative numerical methods can provide the correct solution to the Riemann problem. The study illustrates serious shortfalls in the numerical solution to these problems using standard techniques. By exploring the exact solution, the author suggests how the standard numerical methods can be modified to provide the correct solution to these systems.

Keywords: Nonconservative hyperbolic equations; Multi-phase compressible flow; Combustion; Conservative numerical methods; Riemann problems

1. Introduction

The study has been undertaken to assess the use of standard numerical algorithms to solve nonconservative hyperbolic systems of equations. Shock-capturing methods have been used successfully to resolve flows that develop into discontinuous solutions, such as shocks and contact discontinuities. These have involved conservative forms of the equations for which a whole range of conservative methods of solution have been derived. The methods rely on the conservation form to ensure the correct calculation of shock propagation.

* Fax: +44 1223 765 900.
E-mail address: c.a.lowe@damtp.cam.ac.uk.

0021-9991/$ - see front matter © 2004 Elsevier Inc. All rights reserved.
doi:10.1016/j.jcp.2004.10.023

If the system of equations cannot be written in conservative form, then these are described as nonconservative systems. High-speed multi-phase flows can involve the same features as seen in high-speed single-phase flows, such as the appearance of discontinuous solutions. Multi-phase flows are modelled by nonconservative equations and the study focuses on this type of problem.

The work starts by considering the Riemann problem for a compressible gas in which the cross-sectional area discontinuously changes between the two initial states. The area change can be considered as a discontinuous change in the material porosity. This is a nonconservative problem and effectively describes a multi-phase shock-tube problem in which one of the phases is incompressible and remains stationary. The author has extended the original work by Bdzil et al., that presents the exact solution to this problem for isentropic flows, to a flow that can include discontinuous shock waves. Various numerical methods are applied to the system and these computations are compared with this exact solution; the study displays significant errors in both conservative and nonconservative methods. The analysis suggests that the methods cannot predict the correct jump conditions that apply across the porosity jump. This relates to deficiencies in all the methods that prevent the preservation of correct steady-state solutions. If the numerical methods are modified to apply the correct jump conditions, by exploiting the exact solution and applying this as an "internal" boundary condition, then the conservative methods satisfactorily capture the entire solution.

The author extends these ideas to the complete multi-phase flow problem using the inverse solution methodology described in [2] to provide the exact solution. As seen in the simple study, the numerical solutions are only correctly captured if the correct steady-state jump conditions across porosity jumps are calculated. When the the porosity jump is no longer stationary, and moves at the local velocity of one of the phases, this propagating jump in porosity is described as a "compaction" wave.

2. Review

The model derived by Baer and Nunziato [4] – which will be referred to as the B-N model – describes a gas and solid mixture. Both phases are compressible and this has emerged as the most prominent multi-phase flow model for simulating combustion of energetic materials such as explosives and propellants. It is the numerical solution of this two-phase flow model that is the subject of this study.

Two-phase models include differential terms, in the momentum and energy equations, that mean that the equations cannot be explicitly written in conservative form and therefore cannot be solved in the conventional manner. Baer et al. [5] mathematically analysed the structure of their model and applied various numerical methods of solution. The numerical algorithms involved either are solving the complete system, using the method of lines for example, or splitting the problem into a sequence of two sub-problems that included the solution to a transport equation followed by an ODE integration (to include the effect of algebraic source terms). Similar approaches have been adopted to solve the B-N equations as demonstrated by Bdzil et al. [3,7] and more recently in [2,13].

The same difficulty was encountered in the solution of the Gough model for two-phase flow [8] that describes a mixture of compressible gas and incompressible solid particles – the model adopted in internal ballistic codes, see for example [11,10]. Toro suggested a method of solution for this two-phase flow model based on operator splitting [14]. This was followed by a Roe-type method developed by Sainsaulieu [12], that explicitly considered the consequence of nonconservative terms. However, this analysis was based on the assumption that the porosity associated with the second (non-gas) phase is much smaller than that of the gas-phase – this is not generally the case for applications that adopt the B-N model.

This study will address the physical and numerical effect of nonconservative terms on the solution to a Riemann problem of the B-N equations. Various numerical techniques that may, and indeed have, been used to solve this type of system are computed and compared with the exact solution.

3. Two-phase model

The basic two-phase flow model proposed by Baer and Nunziato [4] is given as follows:

$$\frac{\partial}{\partial t}(\rho\phi) + \frac{\partial}{\partial x}(\rho\phi u) = 0, \tag{1}$$

$$\frac{\partial}{\partial t}(\rho\phi u) + \frac{\partial}{\partial x}(\phi(\rho u^2 + p)) = p\frac{\partial \phi}{\partial x}, \tag{2}$$

$$\frac{\partial}{\partial t}(\phi\rho E) + \frac{\partial}{\partial x}(\phi\rho u(E + pv)) = pu_s\frac{\partial \phi}{\partial x}, \tag{3}$$

$$\frac{\partial}{\partial t}(\rho_s\phi_s) + \frac{\partial}{\partial x}(\rho_s\phi_s u_s) = 0, \tag{4}$$

$$\frac{\partial}{\partial t}(\rho_s\phi_s u_s) + \frac{\partial}{\partial x}(\phi_s(\rho_s u_s^2 + p_s)) = p\frac{\partial \phi_s}{\partial x}, \tag{5}$$

$$\frac{\partial}{\partial t}(\phi_s\rho_s E_s) + \frac{\partial}{\partial x}(\phi_s\rho_S u_s(E_s + p_s v_s)) = pu_s\frac{\partial \phi_s}{\partial x}, \tag{6}$$

$$\frac{\partial \phi_s}{\partial t} + u_s\frac{\partial \phi_s}{\partial x} = 0. \tag{7}$$

The notation $(\,)_s$ denotes the solid phase. Density is written as ρ, porosity is ϕ, specific volume is $v = \rho^{-1}$, u is velocity and p is pressure. The total energy per unit mass is written as E, where

$$E = e + \frac{1}{2}u^2 \tag{8}$$

and e is the specific internal, or intrinsic, thermal energy. Note that the porosities are such that:

$$\phi + \phi_s = 1. \tag{9}$$

The B-N model includes mass, momentum and energy balance equations for both phases and a compaction equation that describes the evolution of the porosity.

All of the algebraic source terms that describe mass, momentum and energy transfer due to combustion, interphase drag and heat transfer plus compaction work terms that appear in the complete B-N system are neglected in this study. The only terms on the right-hand side of Eqs. (1)–(7) that will be retained are the terms:

$$p\frac{\partial \phi}{\partial x}, \quad p\frac{\partial \phi_s}{\partial x},$$

that appear in the momentum equations along with their counterparts:

$$u_s p\frac{\partial \phi}{\partial x}, \quad u_s p\frac{\partial \phi_s}{\partial x},$$

that appear in both energy equations. The presence of the porosity derivative terms seen above in the momentum and energy equations make the system nonconservative and directly effect the wave-structure of the equations. The porosity terms are often described as nozzling terms as they are equivalent to area variation terms seen in the equations that control the flow of compressible gas through a converging nozzle.

The variation in ϕ relates to the variation in cross-sectional area and, in the shock-tube problems that we will be considering, this area changes discontinuously.

4. Two-phase shock-tube problem: solid stationary

Although described as a "two-phase shock-tube" in the literature, the problem actually involves the flow of gas in which the porosity can be different in each part of the chamber, but remains *constant*, that is, the particle bed does not actually move, see Fig. 1. If Eqs. (1)–(7) are considered in which $u_s \equiv 0$ and the solid is further assumed to be *incompressible*, then the following system of equations may be derived, see [3]:

$$\mathbf{U}_t + \mathbf{F}_x(\mathbf{U}) = \mathbf{S}(\mathbf{U}, \phi_x), \tag{10}$$

where

$$\mathbf{U} = \begin{pmatrix} \rho\phi \\ \rho\phi u \\ \rho\phi E \end{pmatrix}, \quad \mathbf{F}(\mathbf{U}) = \begin{pmatrix} \rho\phi u \\ \rho\phi u^2 + \phi p \\ \rho\phi u(E + pv) \end{pmatrix}, \quad \mathbf{S}(\mathbf{U}) = \begin{pmatrix} 0 \\ p\frac{\partial\phi}{\partial x} \\ 0 \end{pmatrix}.$$

Let x_I be the location in the bed in which there is discontinuous change in ϕ; a Riemann problem for this hyperbolic system can be defined using the following initial conditions:

$$\text{for } x < x_I, \quad \rho(x,0) = \rho_L, \quad u(x,0) = u_L, \quad p(x,0) = p_L, \quad \phi(x,t) = 1, \tag{11}$$

$$\text{for } x \geqslant x_I, \quad \rho(x,0) = \rho_R, \quad u(x,0) = u_R, \quad p(x,0) = p_R, \quad \phi(x,t) = \phi_R. \tag{12}$$

The gas is assumed to be ideal, so that

$$e = C_v T = \frac{pv}{(\gamma - 1)}, \quad \eta = C_v \ln pv^{\gamma}, \tag{13}$$

where T is absolute temperature, C_v is specific heat at constant volume, η is entropy and γ is the ratio of specific heats.

Note that Eqs. (11) and (12) provide initial conditions only for the variables ρ, u and p, the condition on ϕ applies for all time. The left-hand region in which $\phi = 1$ will be described as the reservoir, the right-hand region in which $\phi < 1$ is the stationary porous bed and x_I is the interface.

4.1. Exact solution

The exact solution to the above problem for a particular choice of initial conditions was presented in [3] – the solution was isentropic by assuming that $p_R \gg p_L$. Here, this constraint will be removed – in partic-

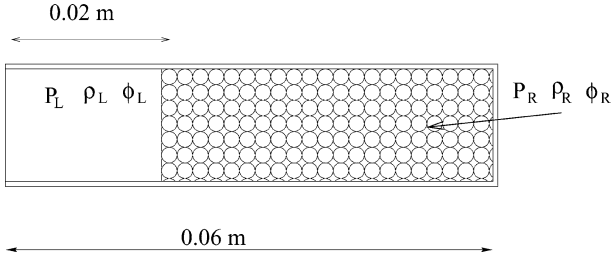

Fig. 1. Schematic of two-phase shock-tube.

ular the nonisentropic formation of shock waves will not be excluded from the solution to the Riemann problem and a slightly different approach will be adopted to provide the exact solution.

Eq. (10) may be rewritten in nonconservative form as:

$$\mathbf{V}_t + \mathbf{A}(\mathbf{V})\mathbf{V}_x = 0,$$

where

$$\mathbf{V} = \begin{pmatrix} \rho \\ u \\ p \\ \phi \end{pmatrix}, \quad \mathbf{A}(\mathbf{V}) = \begin{pmatrix} u & \rho & 0 & \frac{\rho u}{\phi} \\ 0 & u & 1/\rho & 0 \\ 0 & \gamma p & u & \frac{\gamma p u}{\phi} \\ 0 & 0 & 0 & 0 \end{pmatrix}.$$

The eigenvalues for this system are $\lambda_1 = u - a$; $\lambda_2 = u$; $\lambda_3 = u + a$ and $\lambda_4 = 0$. The corresponding eigenvectors are:

$$R_1 = \begin{bmatrix} -\rho/a \\ 1 \\ -\rho a \\ 0 \end{bmatrix}, \quad R_2 = \begin{bmatrix} 1 \\ 0 \\ 0 \\ 0 \end{bmatrix}, \quad R_3 = \begin{bmatrix} \rho/a \\ 1 \\ \rho a \\ 0 \end{bmatrix}, \quad R_4 = \begin{bmatrix} -\rho u^2 \\ u a^2 \\ -\rho a^2 u^2 \\ \phi(u^2 - a^2) \end{bmatrix}, \tag{14}$$

R_1 to R_3 are identical to that of the ordinary Euler equations other than the addition of a final zero entry in the final row which indicates that the porosity does not change across these waves. The Riemann invariants for the final eigenvector provide the following jump conditions across the interface x_I:

$$[\phi\rho u]_- = [\phi\rho u]_+, \tag{15}$$

$$[\eta]_- = [\eta]_+, \tag{16}$$

$$\left[\frac{u^2}{2} + \frac{\gamma p}{\rho(\gamma - 1)}\right]_- = \left[\frac{u^2}{2} + \frac{\gamma p}{\rho(\gamma - 1)}\right]_+. \tag{17}$$

The notation $[\cdot]_-$ and $[\cdot]_+$ describes conditions in the reservoir and porous bed across the interface and η is the entropy of the gas; therefore the solution is isentropic across the interface.

Consequently, use of Eqs. (15)–(17) shows that the jump conditions at the interface satisfy the requirement:

$$M_+^2 = \frac{2}{(\gamma - 1)}\left\{\frac{(\psi^{\gamma-1} - 1)}{\psi^{\gamma-1}(\phi_R^2\psi^2 - 1)}\right\}, \tag{18}$$

where the Mach number is $M = \frac{u}{a}$ and $\psi = (a_+/a_-)^{\frac{2}{\gamma-1}}$.

This is identical to the relation derived in [3] where it is further argued that if $M_-^2 < 1$ and ϕ decreases monotonically in going from the reservoir to the bed, then the flow will accelerate from the reservoir into the bed limited only by the condition $M_+ = 1$ – analogous to the flow within a converging nozzle.

By exploiting this limit and the fact that along the characteristic paths:

$$\frac{\mathrm{d}x}{\mathrm{d}t} = u \pm a$$

the variables:

$$\frac{2a}{\gamma - 1} \pm u$$

are constant, then it can be further shown that:

$$\frac{u_-}{u_+} = \phi_R \psi^{\frac{1}{\gamma}}, \quad u_+ = a_+, \quad u_- = \frac{2 - 2a_-}{\gamma - 1}.$$

The flow structures in the reservoir and the bed are connected via the jump conditions provided above across the interface. The author now departs from the solution described in [3]; it is clear that ϕ only changes across the interface and since we have calculated conditions at either side of the interface, the fluid problem now essentially splits into two Riemann problems for the standard Euler equations. ϕ remains constant throughout the rest of the domain, connected at the interface by conditions (15)–(17) and therefore the following exact solution is proposed:

Solution in the reservoir $x \leqslant x_I$: The solution in the reservoir corresponds to the solution in the region $x \leqslant x_I$ of the Riemann problem of the standard Euler equations (independent of ϕ) in which the pressure, density and velocity to the right of the interface are equal to p_-, ρ_- and u_-, respectively:

$$\mathbf{U}_t + \mathbf{F}_x(\mathbf{U}) = 0,$$

where the initial conditions are:

$$\rho(x,0) = \begin{cases} \rho_L, & x < x_I, \\ \rho_-, & x \geqslant x_I, \end{cases} \quad u(x,0) = \begin{cases} u_L, & x < x_I, \\ u_-, & x \geqslant x_I, \end{cases} \quad p(x,0) = \begin{cases} p_L, & x < x_I, \\ p_-, & x \geqslant x_I. \end{cases} \tag{19}$$

Solution in the bed $x_I \leqslant x$: Similarly, the solution in the bed is given as the solution in region $x_I \leqslant x$ of the standard Riemann problem in which the conditions to the left are given as the jump conditions p_+, ρ_+ and u_+

$$\mathbf{U}_t + \mathbf{F}_x(\mathbf{U}) = 0,$$

where

$$\rho(x,0) = \begin{cases} \rho_+, & x < x_I, \\ \rho_R, & x \geqslant x_I, \end{cases} \quad u(x,0) = \begin{cases} u_+, & x < x_I, \\ u_R, & x \geqslant x_I, \end{cases} \quad p(x,0) = \begin{cases} p_+, & x < x_I, \\ p_R, & x \geqslant x_I. \end{cases} \tag{20}$$

4.2. Test problem

A test problem will be solved using the methodology described in Section 4.1 to provide the exact solution and compared to solutions obtained using a variety of numerical methods that will be described below. The initial conditions are:

$$\begin{aligned} &\phi_L = 1, \quad p_L = 296 \text{ MPa}, \quad T_L = 4000 \text{ K}, \quad u_L = 0 \text{ m/s}, \qquad 0 \leqslant x < 0.02 \text{ m}, \\ &\phi_R = 0.25, \quad p_R = 0.1 \text{ MPa}, \qquad T_R = 300 \text{ K}, \quad u_R = 0 \text{ m/s}, \qquad 0.02 < x \leqslant 0.06 \text{ m} \end{aligned} \tag{21}$$

and $\gamma = 1.23$, $c_V = 1900$ J/(kg K). Solutions to Eq. (10) with initial conditions (21) at time 6.3 μs are presented in Fig. 2. Velocity, density, pressure and entropy are presented; it is clear that only the entropy remains constant across the interface at $x = 0.02$ m. The density and pressure drop across the interface with a corresponding rise in velocity. The four wave pattern that corresponds to this solution is displayed in Fig. 3.

In the reservoir the flow remains isentropic and an expansion wave with head travelling at $\frac{dx}{dt} = u_L - a_L$ and tail travelling at $\frac{dx}{dt} = u^* - a_L^*$ spans the interface $x = x_I$. The density plot displays the contact discontinuity that travels at the local flow velocity u^* and is located at $x \approx 0.044$ m. Ahead of the contact there is a significant increase in entropy that is the consequence of a right travelling shock S_R that is positioned at $x \approx 0.046$ m at $t = 6.3$ μs.

Since this study was initiated, it is apparent that studies by Andrianov and Warnecke [1] have also considered the Riemann problem to this system of equations. In their work it has been found for some choices

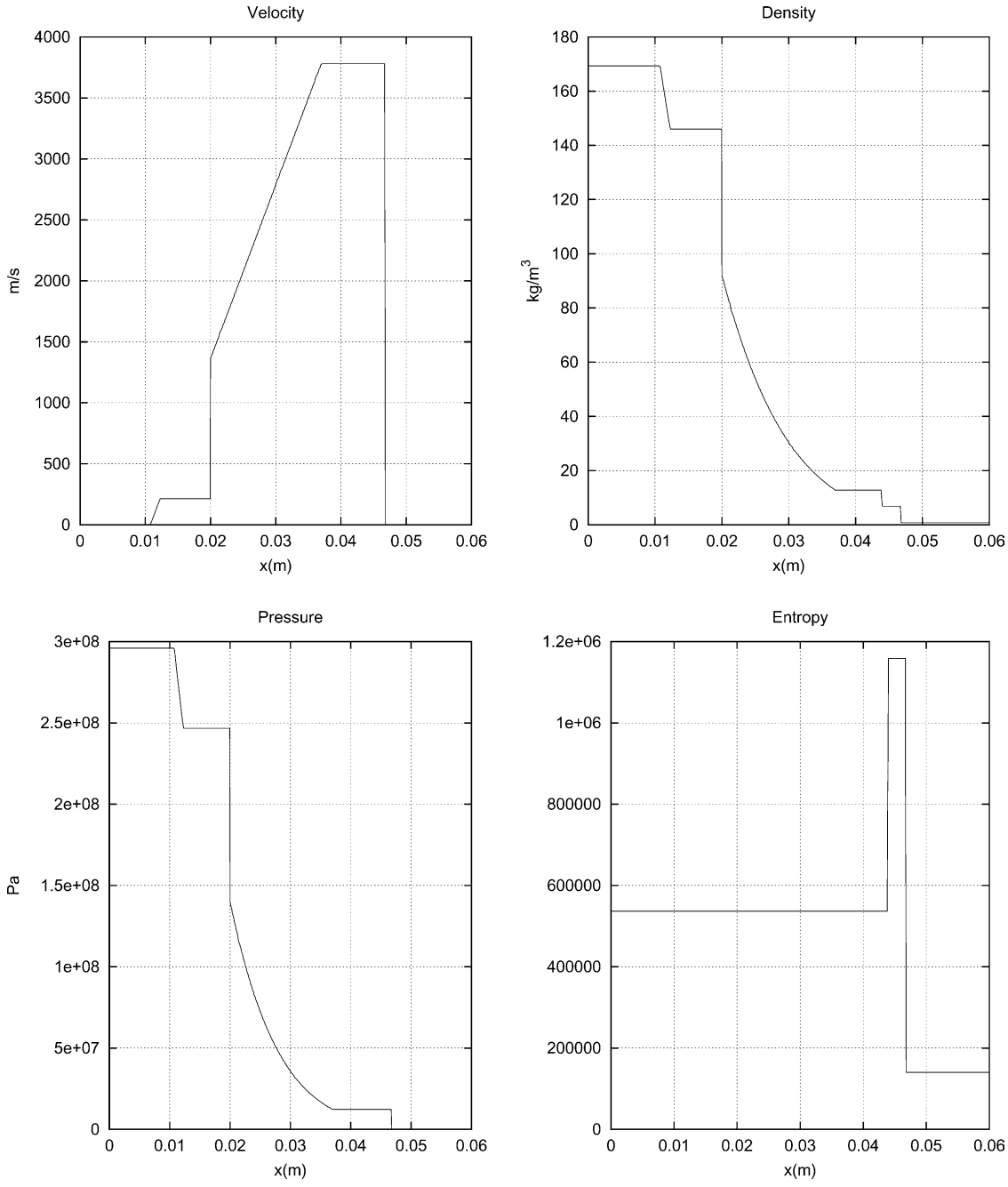

Fig. 2. Exact solution at 6.3 μs.

of initial conditions there is no unique solution to the Riemann problem. However, the type of problem being considered here, that includes a rarefaction wave that actually crosses the porosity jump, was not considered in their study. The author has identified the solution above as the correct physical solution to the problem; work is still in progress on the general nature of these solutions.

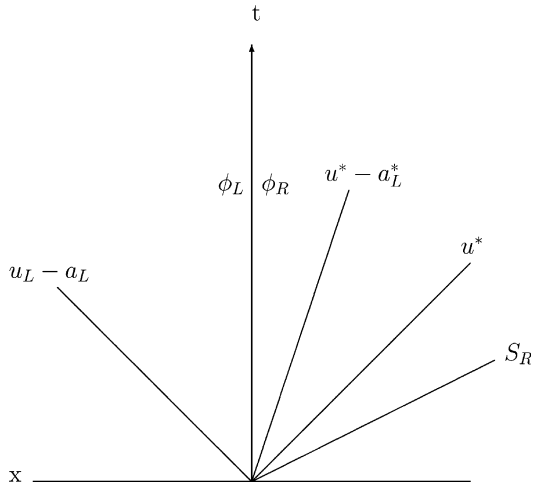

Fig. 3. Wave pattern in the x–t plane.

4.3. Preservation of steady-state solutions

Let us consider the Riemann problem for system (10) that involves initial conditions that by construction must remain in the steady state, that is initial conditions that satisfy:

$$\mathbf{F}_x(\mathbf{U}) \equiv \mathbf{S}(\mathbf{U}, \phi_x) \tag{22}$$

and therefore:

$$\mathbf{U}_t \equiv 0. \tag{23}$$

This is equivalent to requiring that in Eq. (14)

$$\mathbf{A}(\mathbf{V})\mathbf{V}_x \equiv 0.$$

The above condition is effectively what determines jumps conditions (15)–(17). Consequently, the Riemann problem with initial conditions:

$$\rho(x,0) = \begin{cases} \rho_+, & x < x_{\mathrm{I}}, \\ \rho_-, & x \geqslant x_{\mathrm{I}}, \end{cases} \quad u(x,0) = \begin{cases} u_+, & x < x_{\mathrm{I}}, \\ u_-, & x \geqslant x_{\mathrm{I}}, \end{cases} \quad p(x,0) = \begin{cases} p_+, & x < x_{\mathrm{I}}, \\ p_-, & x \geqslant x_{\mathrm{I}} \end{cases} \tag{24}$$

should preserve a steady-state solution. We are interested in studying the case in which $\phi_{\mathrm{L}} \neq \phi_{\mathrm{R}}$: Note, Eqs. (15)–(17) indicate that

$$\Delta p = p_+ - p_- = 0 \Longleftrightarrow \phi_{\mathrm{L}} \equiv \phi_{\mathrm{R}}.$$

Similarly, if $\Delta u = u_+ - u_- = 0$, then:

$$\phi_{\mathrm{L}} \neq \phi_{\mathrm{R}} \Rightarrow \Delta p \neq 0.$$

This implies that steady-state conditions across the compaction wave do not behave as contact discontinuities in standard Euler flows; constant pressure and velocity states are not preserved across the compaction wave.

Various numerical methods will be applied to the steady-state test problem that adopts initial conditions $\mathbf{U}_-$ and $\mathbf{U}_+$ which are precisely the jump conditions found for the test problem in Section 4.2.

5. Numerical methods of solution

Five different methods of solution will be presented here: The first three are standard first-order conservative methods of solution; the Godunov method [15], the FORCE method which is a general centred scheme [15], and a Roe-type method [6]. The former two include the contribution of the nonconservative terms using time-operator splitting whereas the Roe-type method does not use splitting. A solution methodology is then described, for these conservative methods, that uses the exact solution across porosity jumps, described as the "internal boundary" method. A nonconservative method, that also does not require splitting, is also tested [16].

5.1. Conservative methods

Finite-volume methods have been used to solve systems of hyperbolic conservations laws of the form:

$$\mathbf{U}_t + \mathbf{F}_x(\mathbf{U}) = 0. \tag{25}$$

Consider a cell average that is defined for cell i:

$$\mathbf{U}_i^n = \int_{x_{i-1/2}}^{x_{i+1/2}} \mathbf{U}(x, t_n)\, \mathrm{d}x,$$

which is updated in each timestep. Conservative methods update the solution using formula:

$$\mathbf{U}_i^{n+1} = \mathbf{U}_i^n - \frac{\Delta t}{\Delta x}\left(F_{i+1/2}^n - F_{i-1/2}^n\right), \tag{26}$$

where the flux functions $F_{i+1/2}$ and $F_{i-1/2}$ are functions of the initial data $\mathbf{U}_i^n$; the details of these functions are provided by any particular numerical scheme. Some schemes of this type, that have been successfully used to resolve Eq. (25), will be described below.

5.1.1. Conservative methods and time-operator splitting

The well-known Godunov method will use the exact solution of the Riemann problem to the *standard* Euler equations in the solution methodology.

The FORCE method is a general centred scheme that can easily be applied to any conservative hyperbolic system as detailed information about the eigenstructure of the system that is to be solved is not required [15]. The detail of the algorithm is described in Appendix A.

However, the equations in (10) cannot be written in the form seen in Eq. (25). In order to apply conservative methods of solution, the differential terms on the right of Eq. (10) are often rewritten in algebraic form – using simple finite difference approximations – to give a system that is then solved using time-operator splitting. Details of the operator splitting technique are described in Appendix B.

However, note that operator splitting may on occasion mean that problems that should converge to steady-state solutions may not always be correctly resolved. This has prompted the development of nonsplit schemes such as the Roe-type method that will described in the following section.

5.1.2. Unsplit conservative Roe-type method

An unsplit method based on Roe-type decomposition of the flux function [6] is applied to the problem. The general form of the method is outlined in Appendix C and the eigenstructure used to construct the method is identical to that of the standard Euler equations: Define variables $p' \equiv p\phi$ and $\rho' \equiv \rho\phi$; then Eq. (10) may be rewritten as

$$\mathbf{U}'_t + \mathbf{F}_x(\mathbf{U}') = \mathbf{S}(\mathbf{U}', \phi_x), \tag{27}$$

where

$$\mathbf{U}' = \begin{pmatrix} \rho' \\ \rho' u \\ \rho' E \end{pmatrix}, \quad \mathbf{F}(\mathbf{U}) = \begin{pmatrix} \rho' u \\ \rho' u^2 + p' \\ \rho' u (E + p' v') \end{pmatrix}, \quad \mathbf{S}(\mathbf{U}) = \begin{pmatrix} 0 \\ \frac{p'}{\phi} \frac{\partial \phi}{\partial x} \\ 0 \end{pmatrix}.$$

A crucial part of this algorithm relies on choosing a function that approximates the contribution of the nonconservative nozzling term at the intercell boundary that lies along the interface. For instance, the following choice could be made:

$$\left(\frac{p'}{\phi}\frac{\partial \phi}{\partial x}\right)_{\mathrm{I}} \approx \left(\frac{p'}{\phi}\right)_{\mathrm{I}} \frac{(\phi_{i+1} - \phi_i)}{\Delta x} = \frac{(p'_i + p'_{i+1})}{(\phi_i + \phi_{i+1})} \frac{(\phi_{i+1} - \phi_i)}{\Delta x}, \tag{28}$$

where i and $i+1$ are the cells to the left and right of the interface. $(\frac{p'}{\phi})_{\mathrm{I}}$ is the coefficient required to correctly approximate the nonconservative nozzling contribution.

However, is there any reason to believe that such a discretisation will produce the correct steady-state jump conditions across the compaction wave? Can we use information about the known relations that hold across the jump to provide a better estimate for the left-hand side of Eq. (28)?

Recall that the correct discretisation across the interface must preserve the relation $\eta_+ \equiv \eta_-$ along with constant mass flux and enthalpy (see (15)–(17)).

For the standard Euler equations, Roe's method applied to system (27) neglecting all source terms provides the correct jump in mass flux and enthalpy across a typical contact discontinuity:

$$[\rho' u]_- = [\rho' u]_+,$$

$$\left[\frac{u^2}{2} + \frac{\gamma p'}{\rho'(\gamma - 1)}\right]_- = \left[\frac{u^2}{2} + \frac{\gamma p'}{\rho'(\gamma - 1)}\right]_+$$

which are equivalent to Eqs. (15) and (17).

However, for a typical contact discontinuity the flow will remain "isentropic" in the state variable $\eta'(p', \rho')$ which implies that the following jump condition will be satisfied across the porosity jump:

$$\eta' = k\frac{p'}{\rho'^{\gamma}} = k\frac{p\phi}{\rho\phi^{\gamma}} = \eta\phi^{1-\gamma} = \text{constant},$$

where k is constant. This is not equivalent to the flow being isentropic in η, the actual gas entropy. Therefore, the method will preserve the correct relationship across contact discontinuities but without modification will not capture the correct condition across compaction waves.

Therefore to preserve the correct steady-state solution across the compaction wave, we require that the solution remain homentropic in this region. The algorithm must therefore provide a discretisation that preserves the entropy as described. Manipulation of the algorithm for this test problem implies that η will remain constant if:

$$\left(\frac{p'}{\phi}\right)_{\mathrm{I}} (\phi_{i+1} - \phi_i) = \Delta(\phi(\rho u^2 + p)) \tag{29}$$

in which $\Delta(\cdot)$ implies jumps across *the correct steady-state solution*. Both approximations for the source term for the gas-only problems given in Eqs. (28) and (29) will be adopted in the following simulations.

5.1.3. Conservative method with internal boundary

The following method will utilise the conservative methods of solution described above but the effect of the nonconservative terms will not be included by operator splitting as seen in the Godunov and

centred method of Section 5.1.1 or by including extra source-term contributions (as seen in the unsplit Roe-type method of Section 5.1.2). Since the nonconservative terms only present difficulties across the porosity jump, the exact solution provided in Section 4.1 is directly utilised to deal with the behaviour at the interface. The conditions at either side of the interface are set to the exact solution – as constant

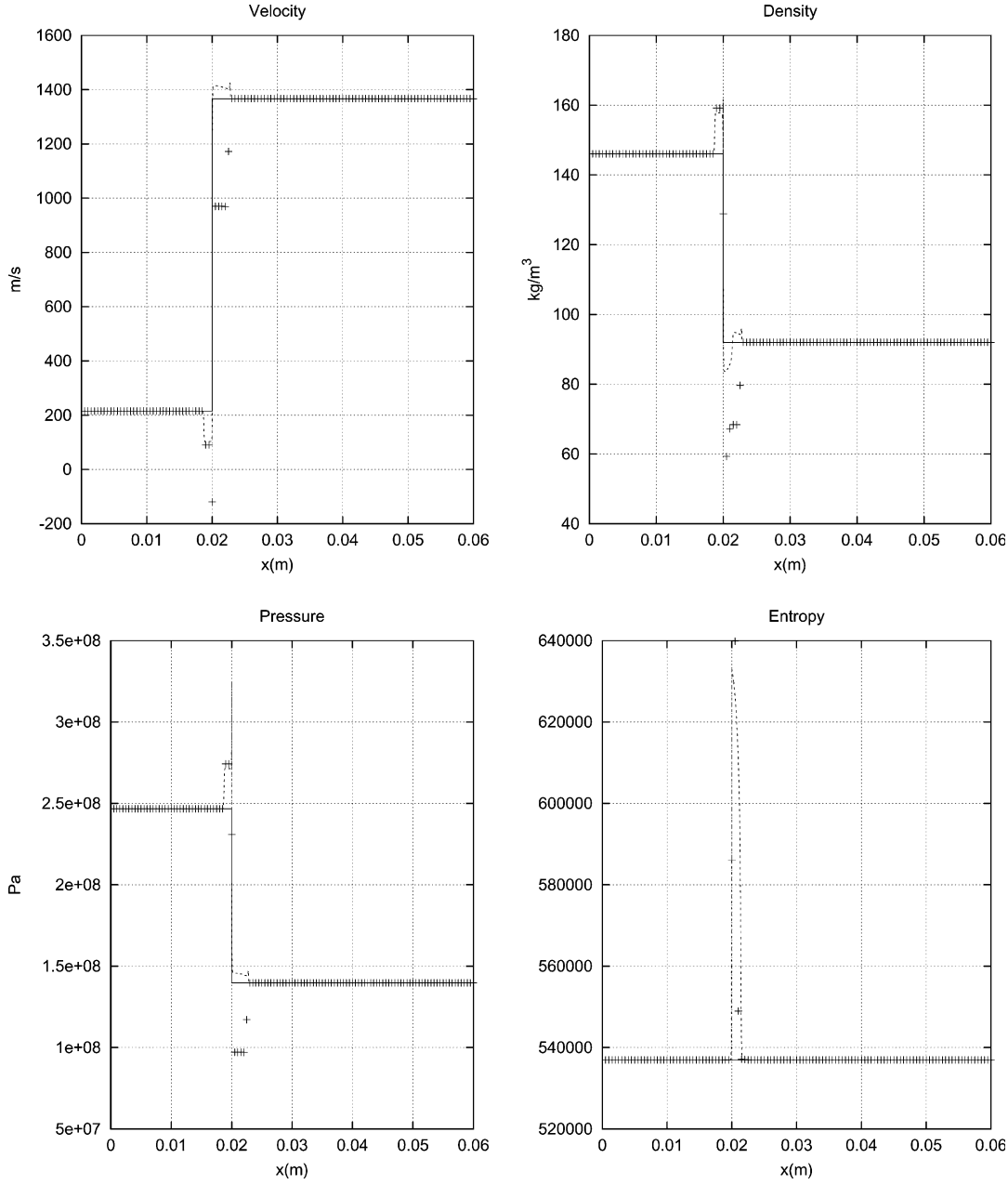

Fig. 4. Split-Godunov and split-conservative centred method: Solution at 1 μs on 12,000 cell mesh: symbol '+' Godunov; dashed line centred; line exact.

internal boundary conditions – and used to construct the intercell flux in the adjacent regions. Therefore, if cell i and cell $i+1$ correspond to the numerical cells at either side of the porosity jump then for all time:

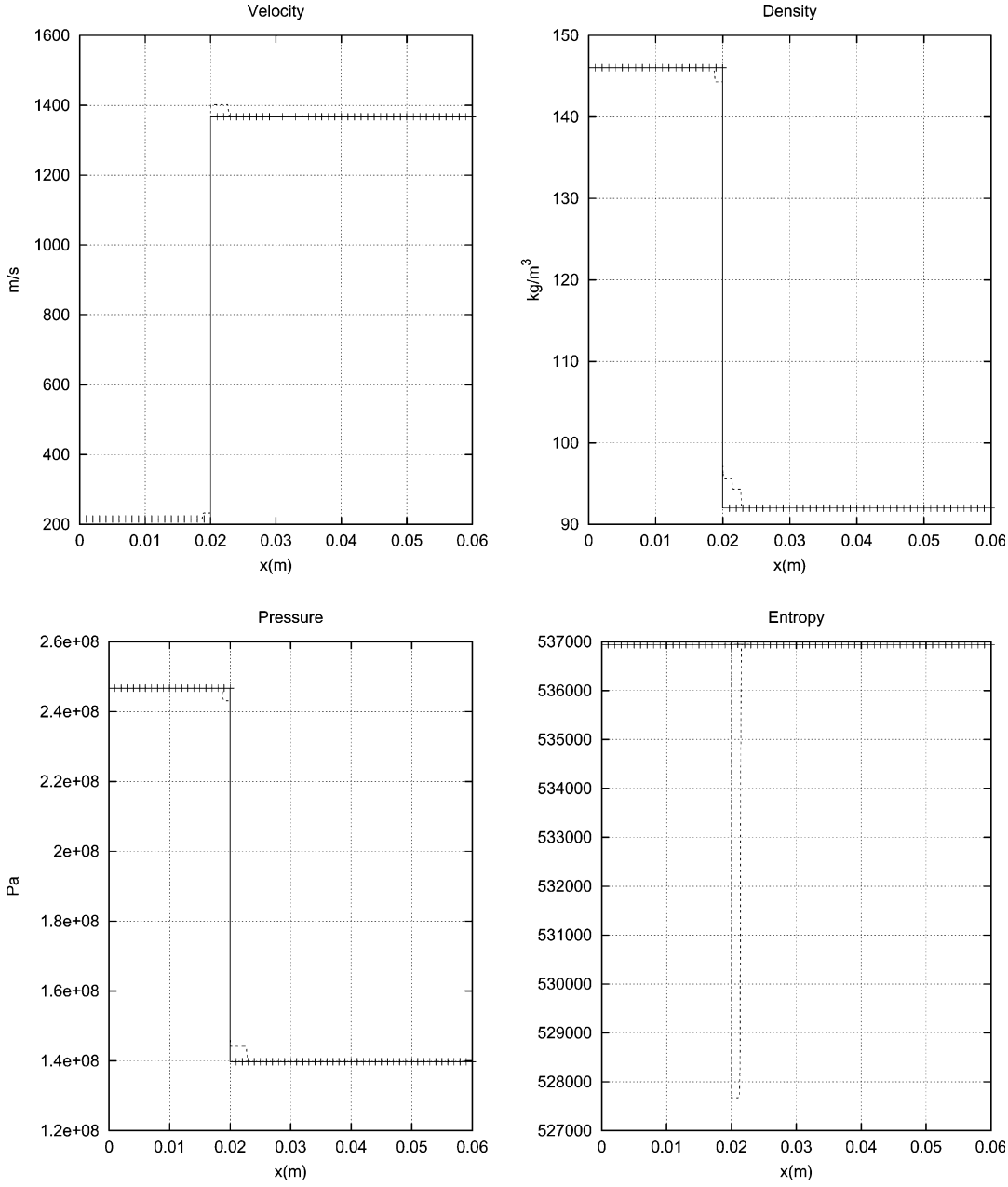

Fig. 5. Unsplit Roe-type method, solution at 1 μs on 12,000 cell mesh: symbol '+' Roe with Eq. (29); dashed line Roe with Eq. (28); line exact.

$$\mathbf{U}_i \equiv \mathbf{U}_-, \quad \mathbf{U}_{i+1} \equiv \mathbf{U}_+.$$

Since by construction this method has been *designed* to ensure that steady-state conditions at either side of the porosity jump remain steady, there is no value in simulating the steady-state problem as this will be perfectly captured.

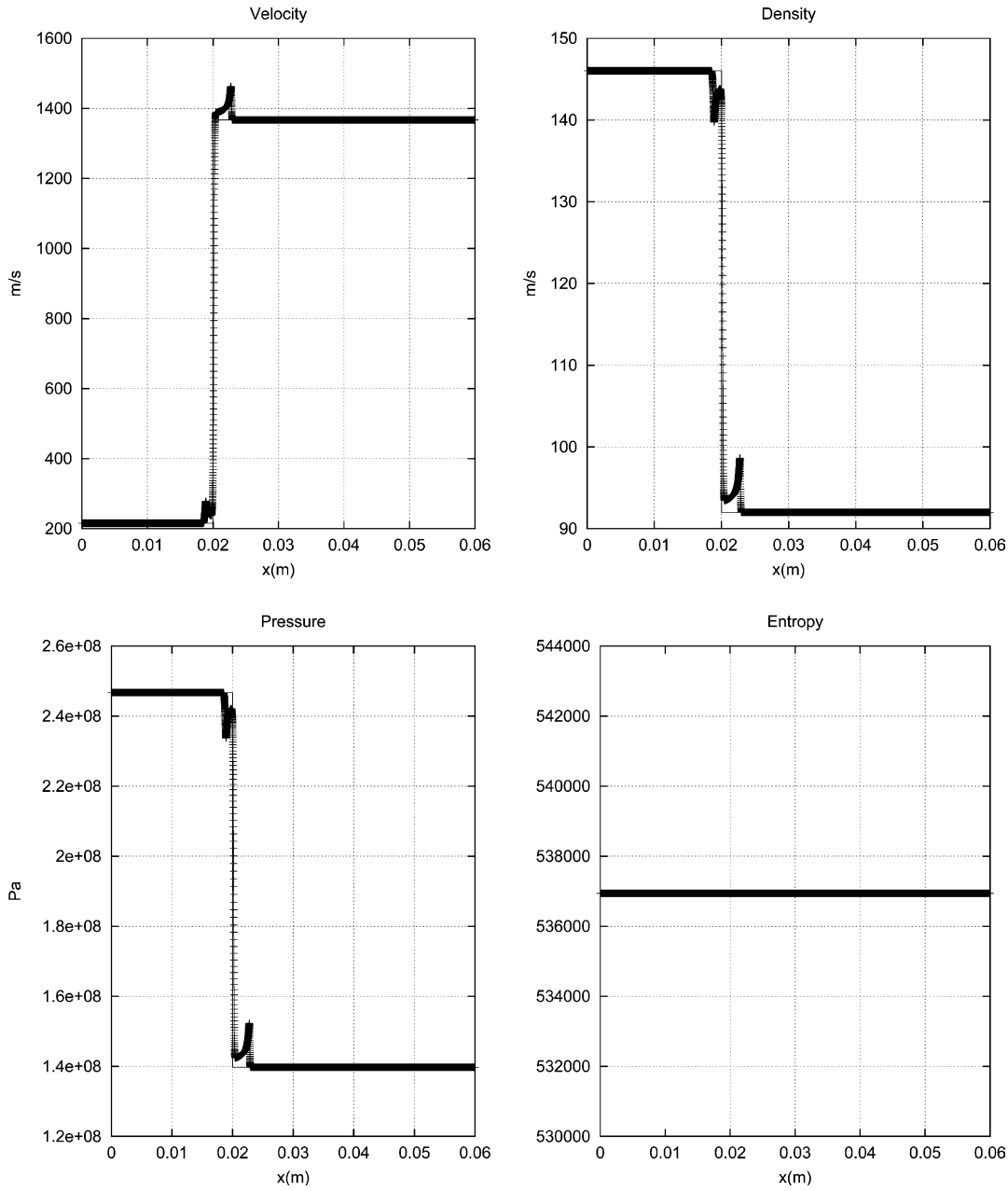

Fig. 6. Nonconservative method, solution at 1 μs on 12,000 cell mesh: symbol '+' numerical; line exact.

Note that the internal boundary method may be applied to any conservative method and it has been used in the construction of higher-order solutions. If the Godunov method is selected, then the solution methodology is equivalent to the Godunov-type method proposed by Andrianov and Warnecke [1] and to the Godunov-type method derived by Greenberg et al. [9], that was applied to a similar problem.

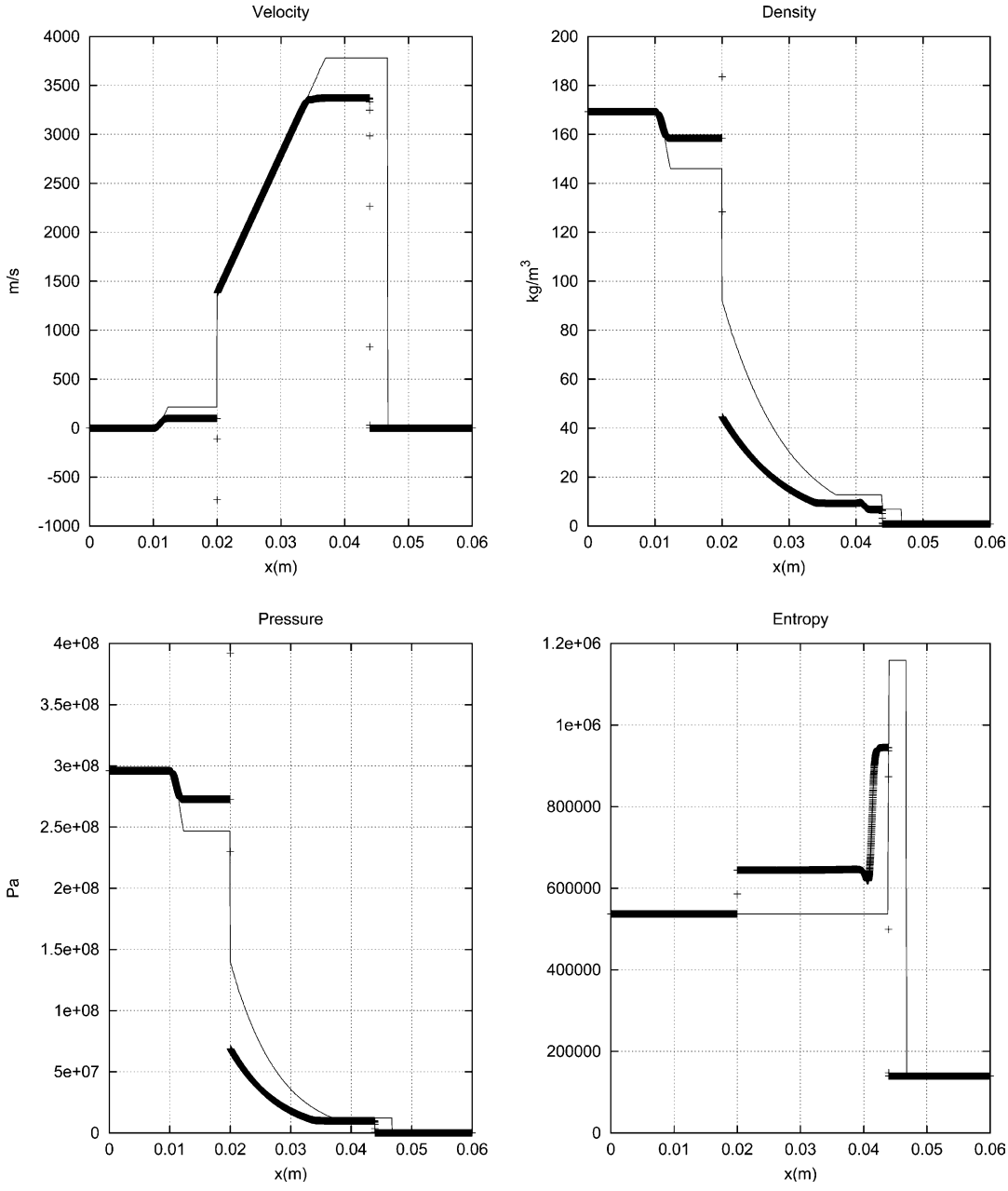

Fig. 7. Split-Godunov method, solution at 6.3 μs on 12,000 cell mesh: symbol '+' numerical; line exact.

5.2. Nonconservative method

A nonconservative first-order centred method of solution, as presented in [16], will be employed to solve the equations. This is actually the nonconservative analogue of the FORCE method described in Section 5.1.1, details are given in Appendix D. It is well known that solutions of nonconservative equations will not capture the propagation of shock waves correctly due to the fact that mass, momentum and energy are not explicitly conserved across jumps. However, the objective of applying this type of method to this problem is to test whether the methods *are* capable of accurately predicting nonconservative jump conditions. Only the solution in isentropic (shockless) regions will be plotted.

5.3. Results for two-phase shock-tube problem: stationary solid

5.3.1. Steady-state problem

Figs. 4–6 present the solutions obtained by using the methods described in Sections 5.1 and 5.2 (apart from the internal boundary method since, by construction, this will always produce the correct solution for this problem) for the steady-state problem described in Section 4.3.

Both conservative methods that employ operator splitting, seen in Fig. 4, do not preserve steady-state conditions. There is a large increase in entropy across the porosity jump and low amplitude disturbances emerge that are clearly visible in the plots for density, velocity and pressure.

Fig. 5 describes solutions produced using the unsplit Roe-method. Two numerical solutions have been plotted that correspond to the discretisation of the source term given in Eqs. (28) and (29). The discretisation given by Eq. (28) introduces changes in the entropy and slight glitches in all other flow variables. The discretisation given by Eq. (29) preserves constant η and preserves steady-state conditions.

Finally, the solution produced by the nonconservative method can be seen in Fig. 11. The method does preserve constant η; nevertheless, small amplitude wave disturbances are still apparent in the density, velocity and pressure.

Out of all the numerical methods considered only the Roe-type method, that chooses a discretisation of the source term that enforces constant entropy across the porosity jump, is entirely successful at achieving the correct solution.

5.3.2. Time-dependent problem

Figs. 7–10 present the solutions obtained by using the methods described in Sections 5.1 and 5.2, respectively, for the time-dependent problem detailed in Section 4.2.

The solutions obtained using conservative methods and operator splitting, see Figs. 7 and 8, do not correctly predict the jump conditions at $x = 0.02$ m. This is not entirely surprising considering the results of the previous section. The flow conditions are not captured in the bed or the reservoir at the interface. Notice that in both Figs. 7 and 8, the entropy is not constant across the interface. The inaccuracy at the interface has direct repercussions on the rest of the flow field and consequently the solution in the right-hand domain illustrates a shock and contact travelling at incorrect speeds and of incorrect strength.

Two solutions of the Roe-type method are illustrated in Fig. 9. As in the previous section, discretisations given in Eq. (28) and (29) have been used. The solution corresponding to Eq. (29) displays excellent agreement with the exact solution and preserves constant entropy across the porosity jump. The solution corresponding to Eq. (28) shows some variation from the exact solution at the interface and there is also a slight decrease in entropy.

Fig. 10 displays the solution in which the exact solution at the interface is utilised in the numerical method to provide an internal boundary. It is clear that the complete solution is captured extremely well and is completely isentropic across the interface.

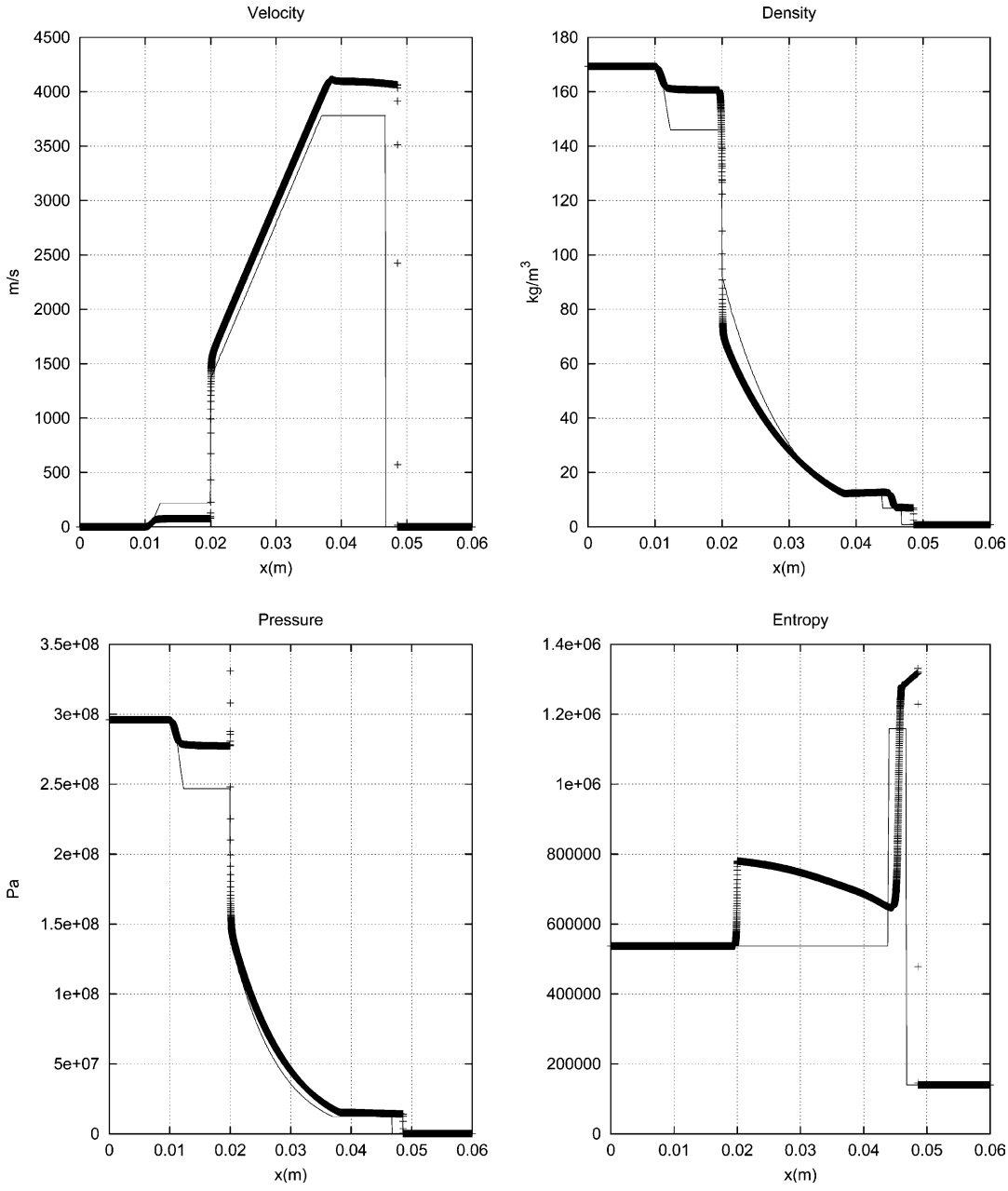

Fig. 8. Split-conservative centred method, solution at 6.3 μs on 12,000 cell mesh: symbol '+' numerical; line exact.

The solution provided by the first-order nonconservative method is seen in Fig. 11. Note that the solution in the region of the shock has been removed as it is known that this type of method will not be able to capture these features correctly. The flow across the interface is isentropic but the solution is quite smeared. This is directly related to the fact that, unlike the previous methods of solution that do not require any

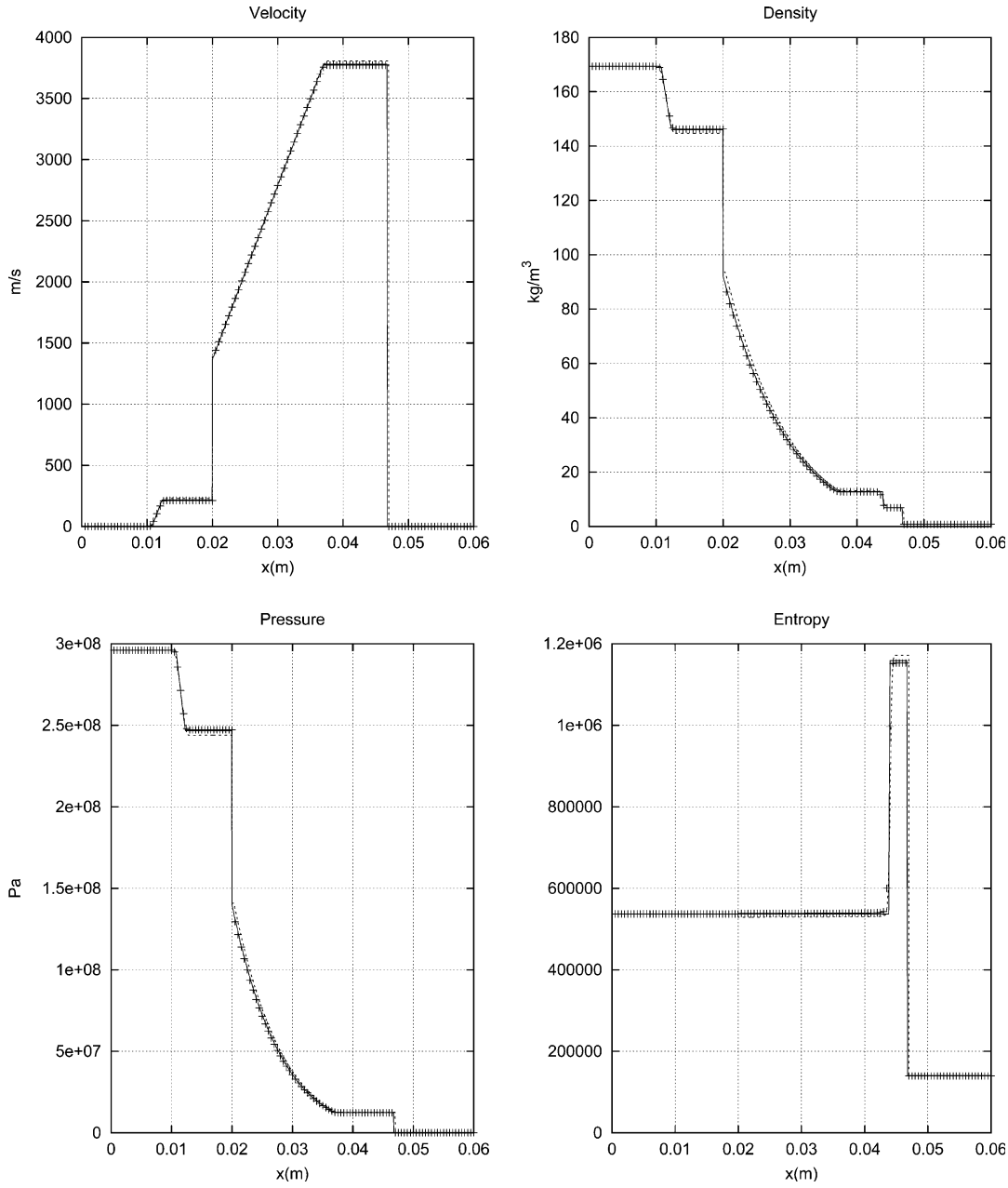

Fig. 9. Unsplit Roe-type method, solution at 6.3 μs on 12,000 cell mesh: symbol '+' Roe with Eq. (29); dashed line Roe with Eq. (28); line exact.

update of ϕ, the nonconservative method updates ϕ at each time-step. This produces smearing across the porosity interface. The nonconservative method can accurately enforce the isentropy across the jump at the interface. However, the inability of the method to maintain steady-state jump conditions implies that

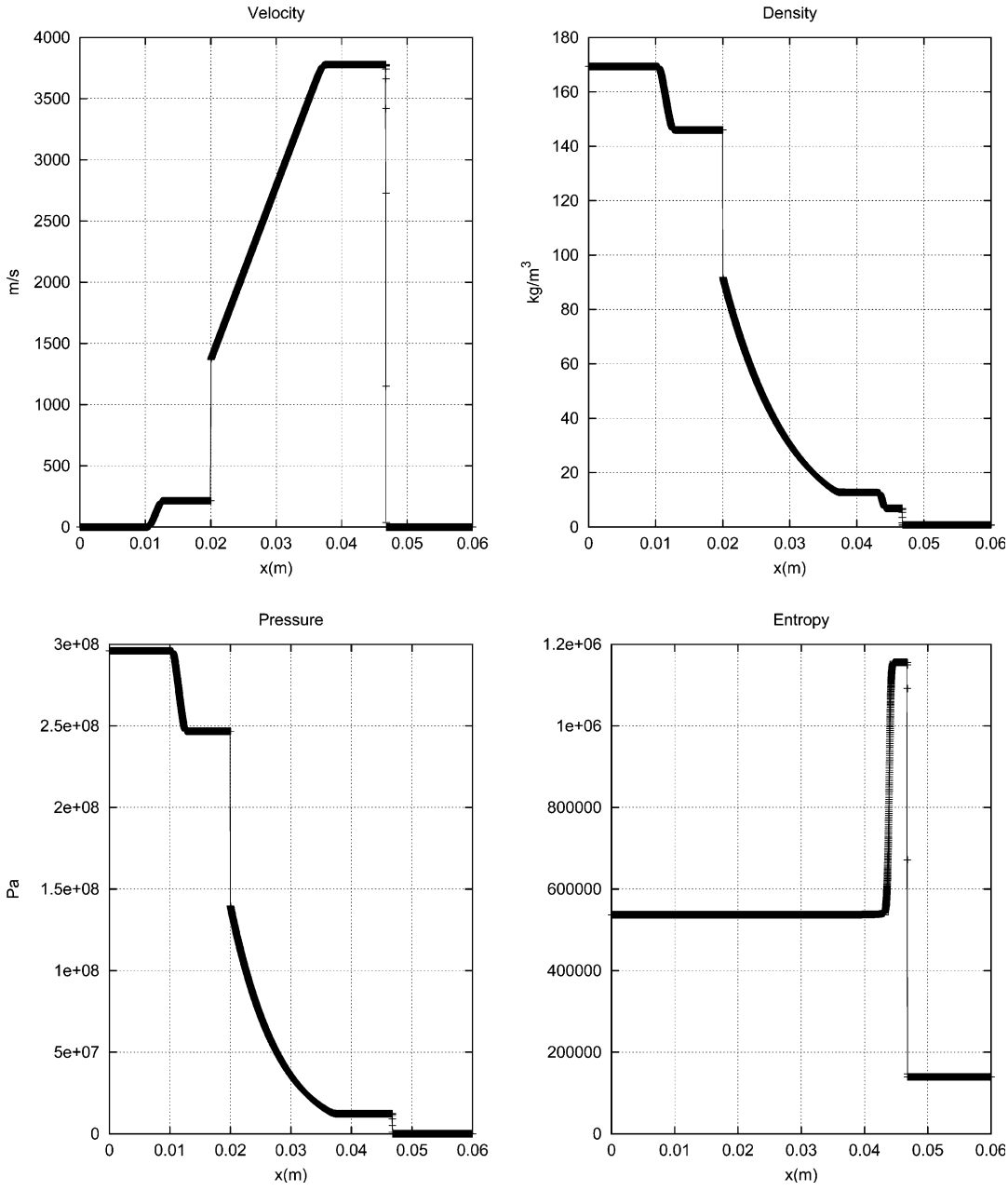

Fig. 10. Godunov method with internal boundary, solution at 6.3 μs on 12,000 cell mesh: symbol '+' numerical; line exact.

the method may still need development to successfully resolve this type of problem – we will see in the next section that this deficiency can be more apparent in the final solution.

We will now use some of the above numerical methods to solve the complete set of two-phase flow equations.

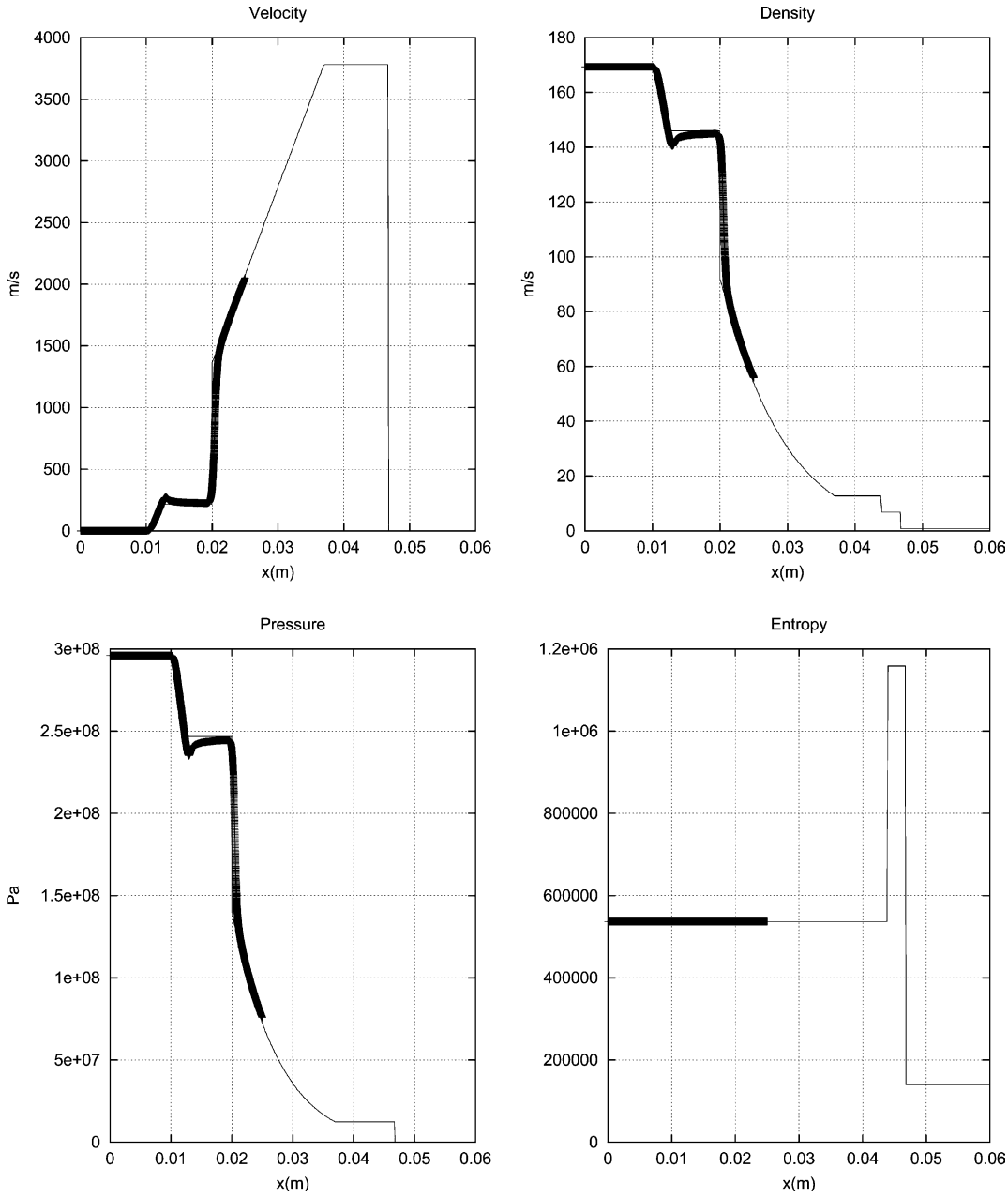

Fig. 11. Nonconservative method, solution at 6.3 μs on 12,000 cell mesh: thick line numerical; thin line exact.

6. Two-phase shock-tube problem

We will now revert to the complete two-phase problem in which the second phase is also fully compressible:

$$\mathbf{U}_t + \mathbf{F}_x(\mathbf{U}) = \mathbf{S}(\mathbf{U}, \phi_x), \tag{30}$$

where

$$\mathbf{U} = \begin{pmatrix} \rho\phi \\ \rho\phi u \\ \rho\phi E \\ \rho_s\phi_s \\ \rho_s\phi_s u_s \\ \rho_s\phi_s E_s \\ \rho_s \end{pmatrix}, \quad \mathbf{F}(\mathbf{U}) = \begin{pmatrix} \rho\phi u \\ \rho\phi u^2 + \phi p \\ \rho\phi u(E + pv) \\ \rho_s\phi_s u_s \\ \rho_s\phi_s u_s^2 + \phi_s p_s \\ \rho_s\phi_s u_s(E_s + p_s v_s) \\ \rho_s u_s \end{pmatrix}, \quad \mathbf{S}(\mathbf{U}) = \begin{pmatrix} 0 \\ p\frac{\partial\phi}{\partial x} \\ u_s p\frac{\partial\phi}{\partial x} \\ 0 \\ p\frac{\partial\phi_s}{\partial x} \\ u_s p\frac{\partial\phi_s}{\partial x} \\ 0 \end{pmatrix}.$$

In Eq. (30), the porosity evolution equation has been rewritten in a conservative form involving the solid density. By doing so the left-hand side of the above system is a fully conservative system that closely resembles the Euler equations for each individual phase. All nonconservative terms are written on the right.

A shock-tube problem, with constant left and right conditions across x_I, may then be defined as Eq. (30) with initial conditions:

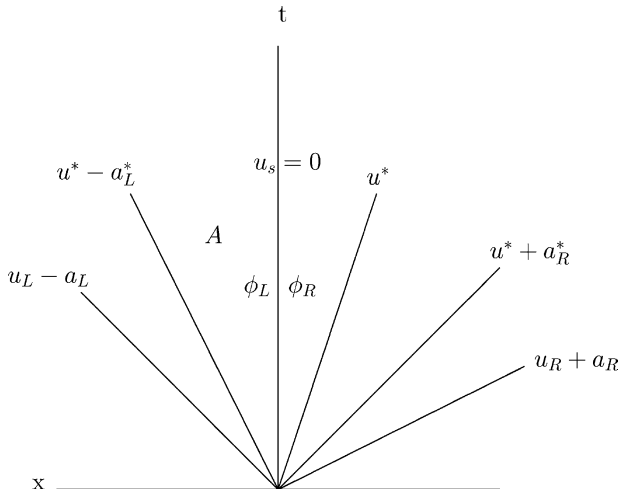

Fig. 12. Inverse solution of the Riemann problem for two-phase flow: solid steady-state solution.

Table 1
Initial conditions for a two-phase flow problem

Gas	Solid
$\phi_L = 0.7$	$\phi_{sL} = 0.3$
$\phi_R = 0.3$	$\phi_{sR} = 0.7$
$u_L = -0.74$ m/s	$u_{sL} = 0$ m/s
$u_R = 0.88$ m/s	$u_{sR} = 0$ m/s
$p_L = 6.68$ Pa	$p_{sL} = 0.35$ Pa
$p_R = 1.75$ Pa	$p_{sR} = 1.22$ Pa
$\rho_L = 5.92$ kg/m^3	$\rho_{sL} = 0.55$ kg/m^3
$\rho_R = 1.94$ kg/m^3	$\rho_{sR} = 1.34$ kg/m^3

$$\text{for } x < x_{\mathrm{I}}, \quad \begin{cases} \rho(x,0) = \rho_{\mathrm{L}}, & u(x,0) = u_{\mathrm{L}}, \quad p(x,0) = p_{\mathrm{L}}, \quad \phi(x,0) = \phi_{\mathrm{L}}, \\ \rho_{\mathrm{s}}(x,0) = \rho_{\mathrm{sL}}, & u_{\mathrm{s}}(x,0) = u_{\mathrm{sL}}, \quad p_{\mathrm{s}}(x,0) = p_{\mathrm{sL}}, \quad \phi_{\mathrm{s}}(x,0) = \phi_{\mathrm{sL}}, \end{cases}$$

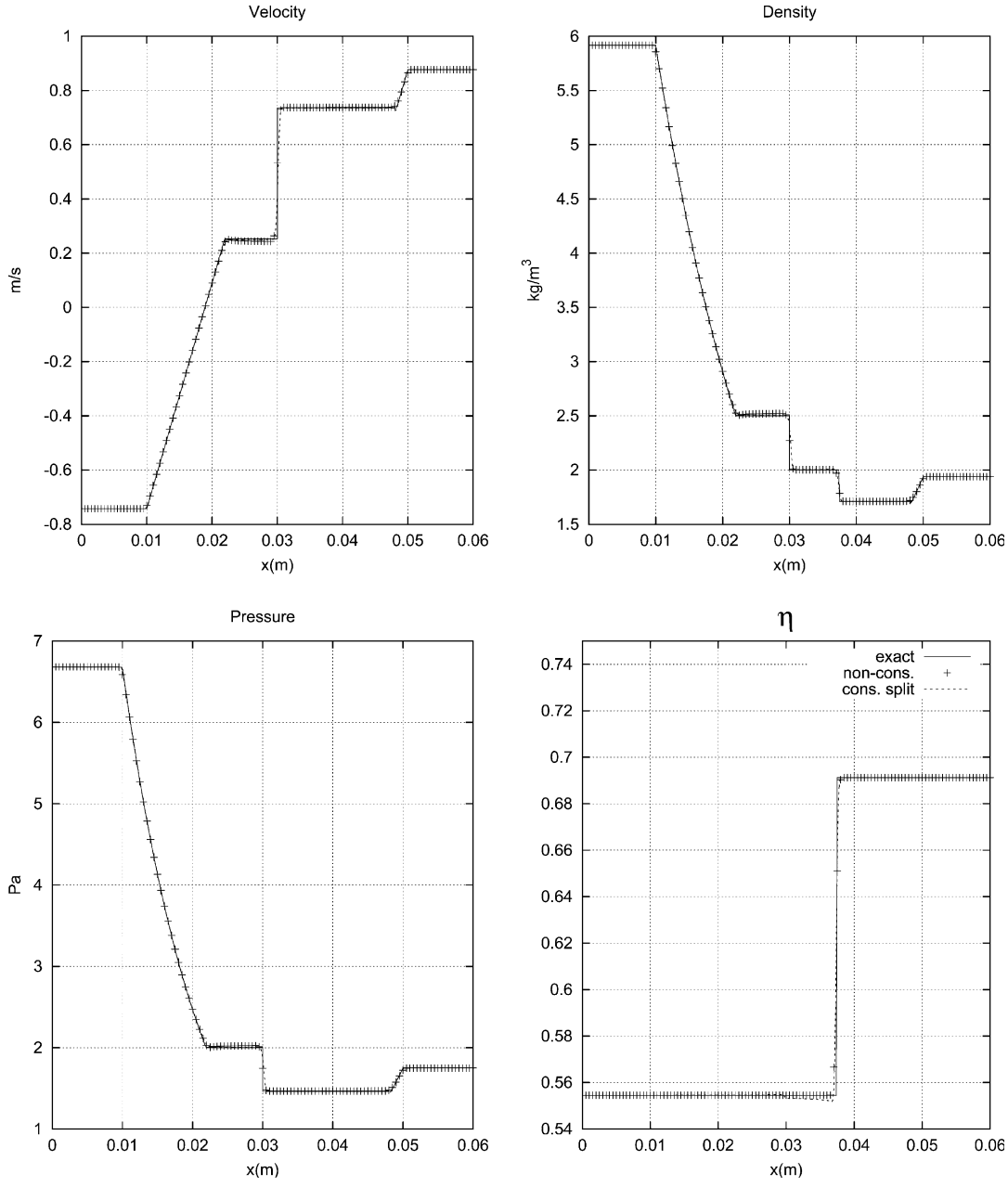

Fig. 13. Gas-phase solution at 0.01 s: split-conservative centred and nonconservative solution on 12,000 cell mesh.

$$\text{for } x \geqslant x_{\mathrm{I}}, \quad \begin{cases} \rho(x,0) = \rho_{\mathrm{R}}, \quad u(x,0) = u_{\mathrm{R}}, \quad p(x,0) = p_{\mathrm{R}}, \quad \phi(x,0) = \phi_{\mathrm{R}}, \\ \rho_{\mathrm{s}}(x,0) = \rho_{\mathrm{sR}}, \quad u_{\mathrm{s}}(x,0) = u_{\mathrm{sR}}, \quad p_{\mathrm{s}}(x,0) = p_{\mathrm{sR}}, \quad \phi_{\mathrm{s}}(x,0) = \phi_{\mathrm{sR}}. \end{cases}$$

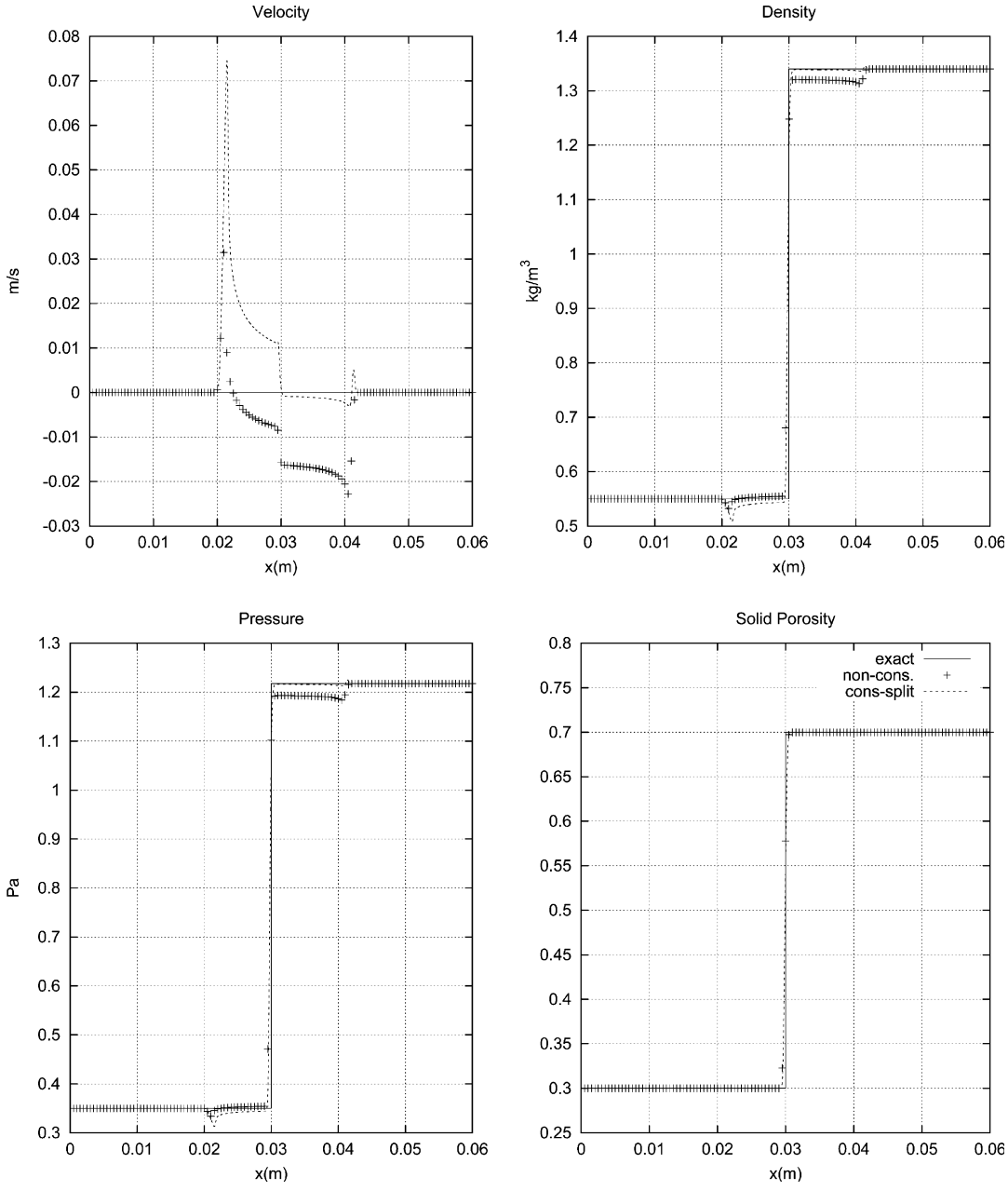

Fig. 14. Solid-phase solution at 0.01 s: split-conservative centred and nonconservative solution on 12,000 cell mesh.

Before proceeding to deal with the full system of equations with nonconservative nozzling terms it is useful, as a validation exercise, to test the various numerical methods on the fully conservative system before proceeding to nonconservative systems.

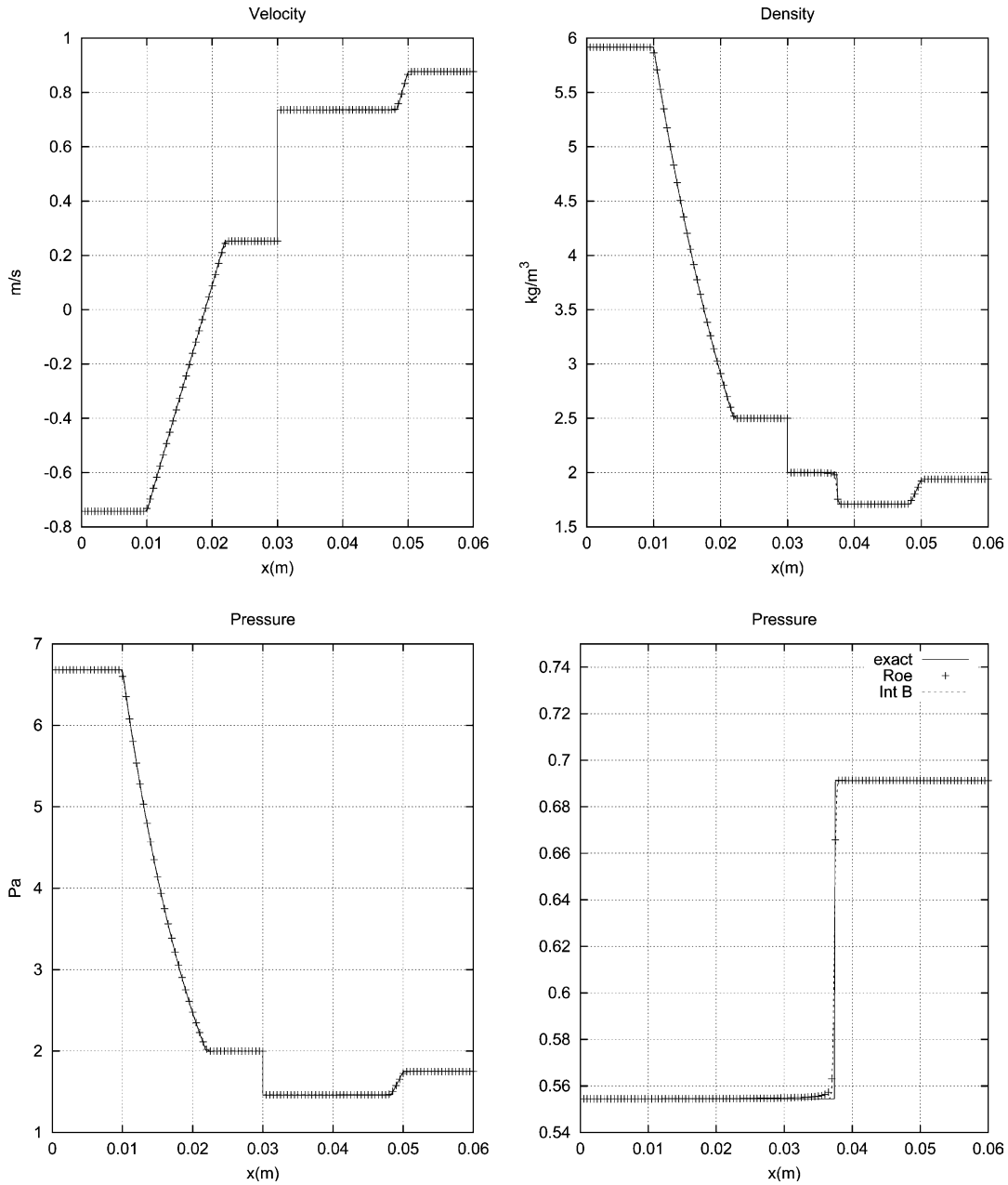

Fig. 15. Gas-phase solution at 0.01 s: internal boundary and unsplit Roe solution on 12,000 cell mesh.

By rewriting the system with $\rho' = \phi\rho$; $\rho'_s = \phi_s\rho_s$; $p' = \phi p$ and $p'_s = \phi_s p_s$ and settings $\mathbf{S}(\mathbf{U}) \equiv 0$ it is easy to show that we derive two systems of Euler equations for each phase along with:

$$\frac{\partial \rho'_s \psi}{\partial t} + \frac{\partial \rho'_s \psi u_s}{\partial x} = 0,$$

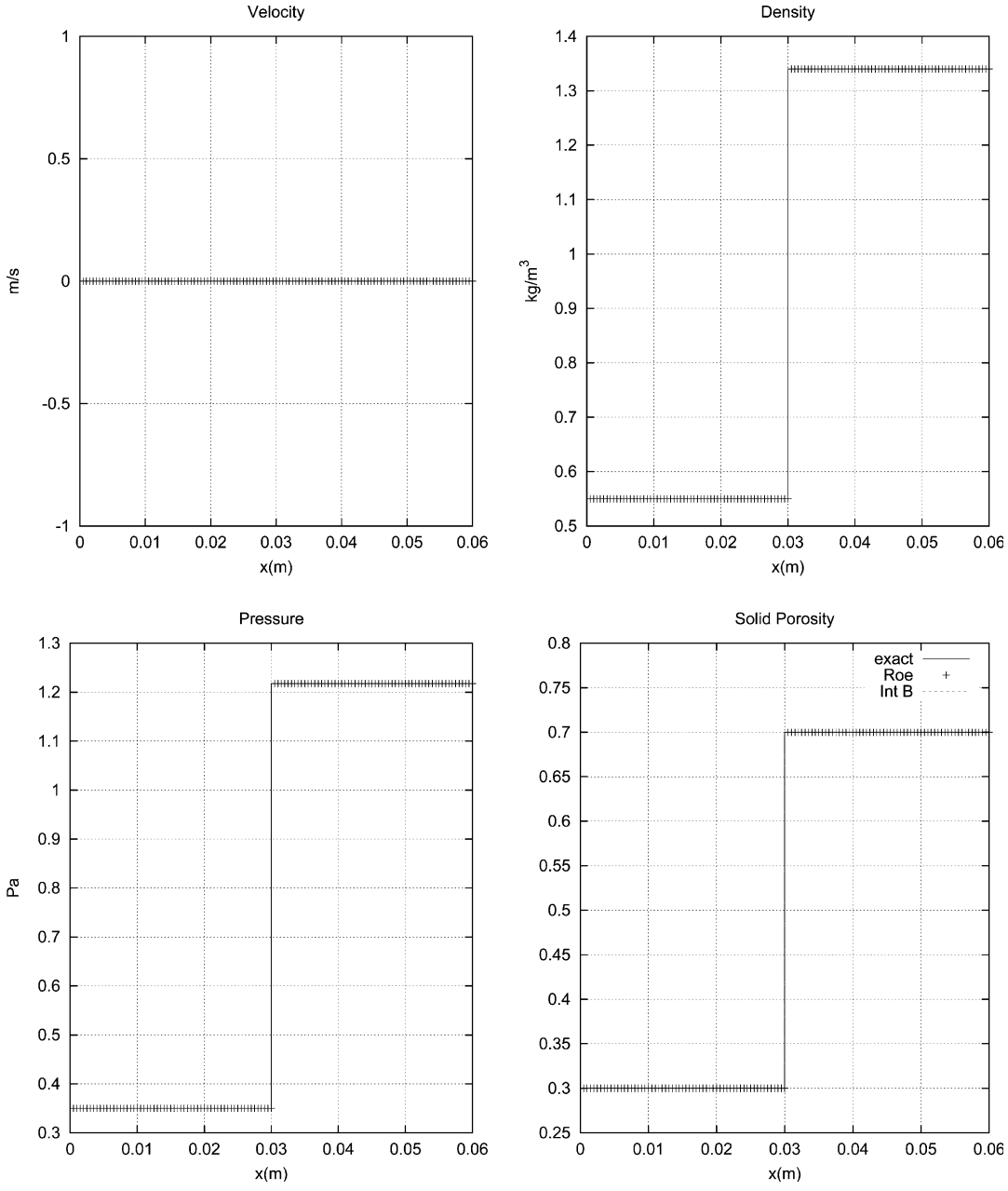

Fig. 16. Solid-phase solution at 0.01 s: internal boundary centred and unsplit Roe solution on 12,000 cell mesh.

where $\psi = 1/\phi_s$. In this case the eigenstructure of the problem is identical to the Euler equations with wave-speeds $u + a$; u; $u - a$; $u_s + a_s$; u_s; u_s; $u_s - a_s$, where a and a_s are the sound speeds of the gas and solid, respectively. The repeated eigenvalue u_s relates to the variable ψ that is passively advected by the local velocity u_s. Again for simplicity we will assume that each phase has an ideal equation of state with ratio of specific heats γ and γ_s which will both be set such that:

$$\gamma = \gamma_s = 1.4.$$

From this an exact solution can be derived for the two-phase system. Most importantly in the absence of shock waves the flow is "isentropic" such that:

$$\frac{p'}{\rho'^{\gamma}} \equiv \frac{p}{\rho^{\gamma}}\phi^{1-\gamma} = \Phi(\phi)\eta = \text{constant}, \quad \frac{p'_s}{\rho'^{\gamma}_s} \equiv \frac{p_s}{\rho^{\gamma_s}_s}\phi_s^{1-\gamma_s} = \Phi(\phi_s)\eta_s = \text{constant}, \tag{31}$$

which actually implies that the relationship between the pure phase density ρ and pressure p is *not* isentropic if the nozzling term is neglected.

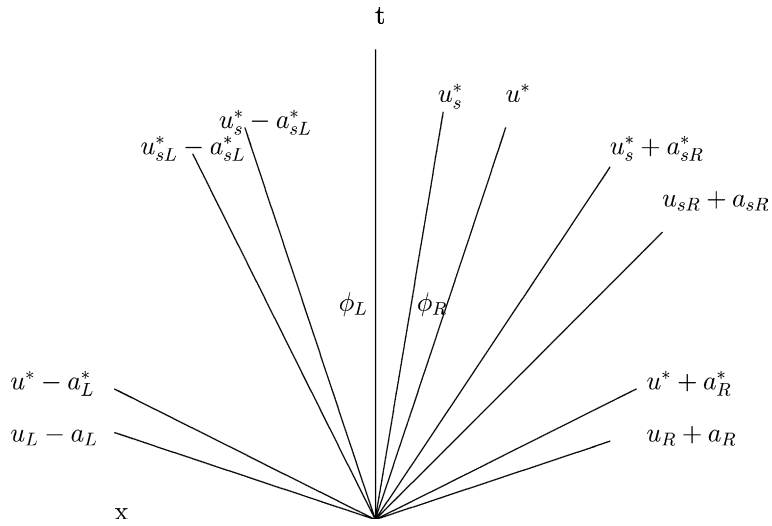

Fig. 17. Inverse solution of the Riemann problem for two-phase flow: four expansion waves and two contacts.

Table 2
Initial conditions for a two-phase flow problem

Gas	Solid
$\phi_L = 0.7$	$\phi_{sL} = 0.3$
$\phi_R = 0.3$	$\phi_{sR} = 0.7$
$u_L = -0.75$ m/s	$u_{sL} = -0.0553$ m/s
$u_R = 0.86$ m/s	$u_{sR} = -0.115$ m/s
$p_L = 6.36$ Pa	$p_{sL} = 0.3527$ Pa
$p_R = 1.87$ Pa	$p_{sR} = 1.1234$ Pa
$\rho_L = 5.71$ kg/m^3	$\rho_{sL} = 0.553$ kg/m^3
$\rho_R = 2.02$ kg/m^3	$\rho_{sR} = 1.264$ kg/m^3

The conservative centred method, Roe-type method and nonconservative centred method, employed in Section 5, are extended to solve the larger system of equations: The full eigenstructure that is used to devise the Roe solution is detailed in Appendix E along with details of the nonconservative form.

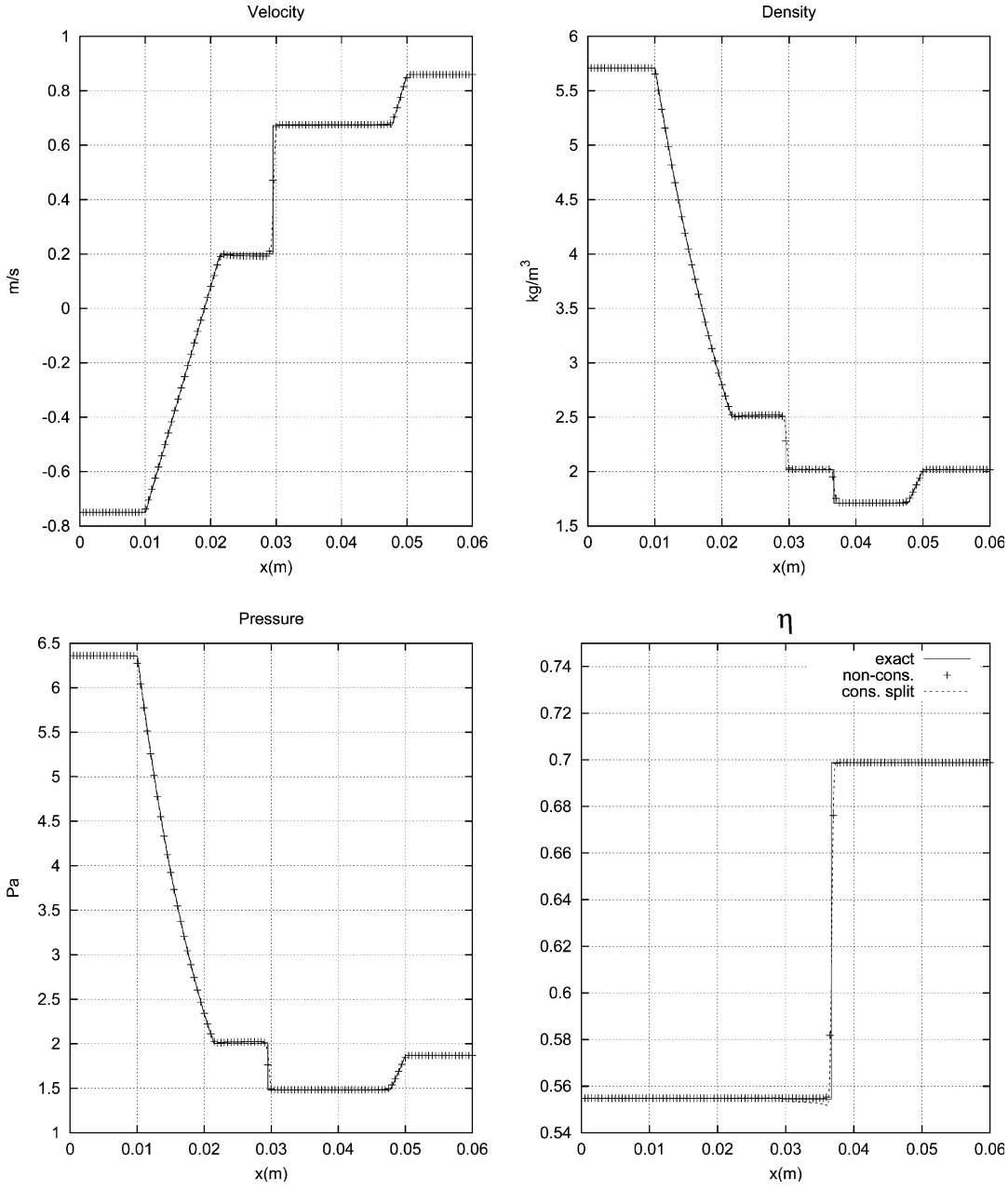

Fig. 18. Gas-phase solution at 0.01 s: split-conservative centred and nonconservative solution on 12,000 cell mesh.

6.1. Effect of nozzling terms

We now consider the exact solution to the complete two-phase system; an "inverse" solution methodology was suggested in [2]: This involves fixing the desired combination of waves and wave-speeds and by

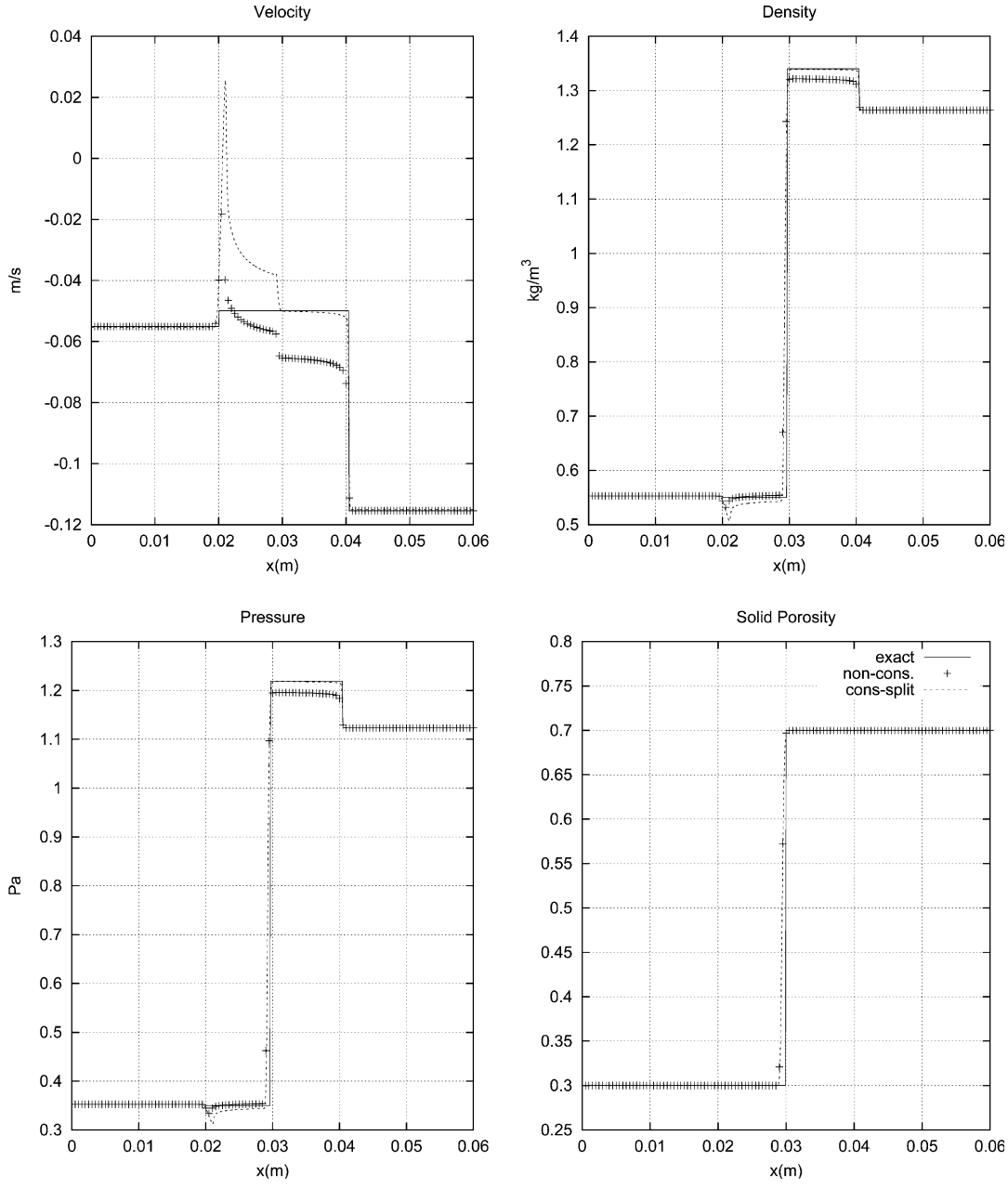

Fig. 19. Solid-phase solution at 0.01 s: split-conservative centred and nonconservative solution on 12,000 cell mesh.

using the necessary jump conditions and Riemann invariants, determining which initial conditions would provide such a solution.

It has been shown in [5] that the compaction wave is linearly degenerate and the Riemann invariants are such that across the compaction wave the solid velocity u_s and the entropy of the gas and solid remain constant. The complete jump conditions are such that:

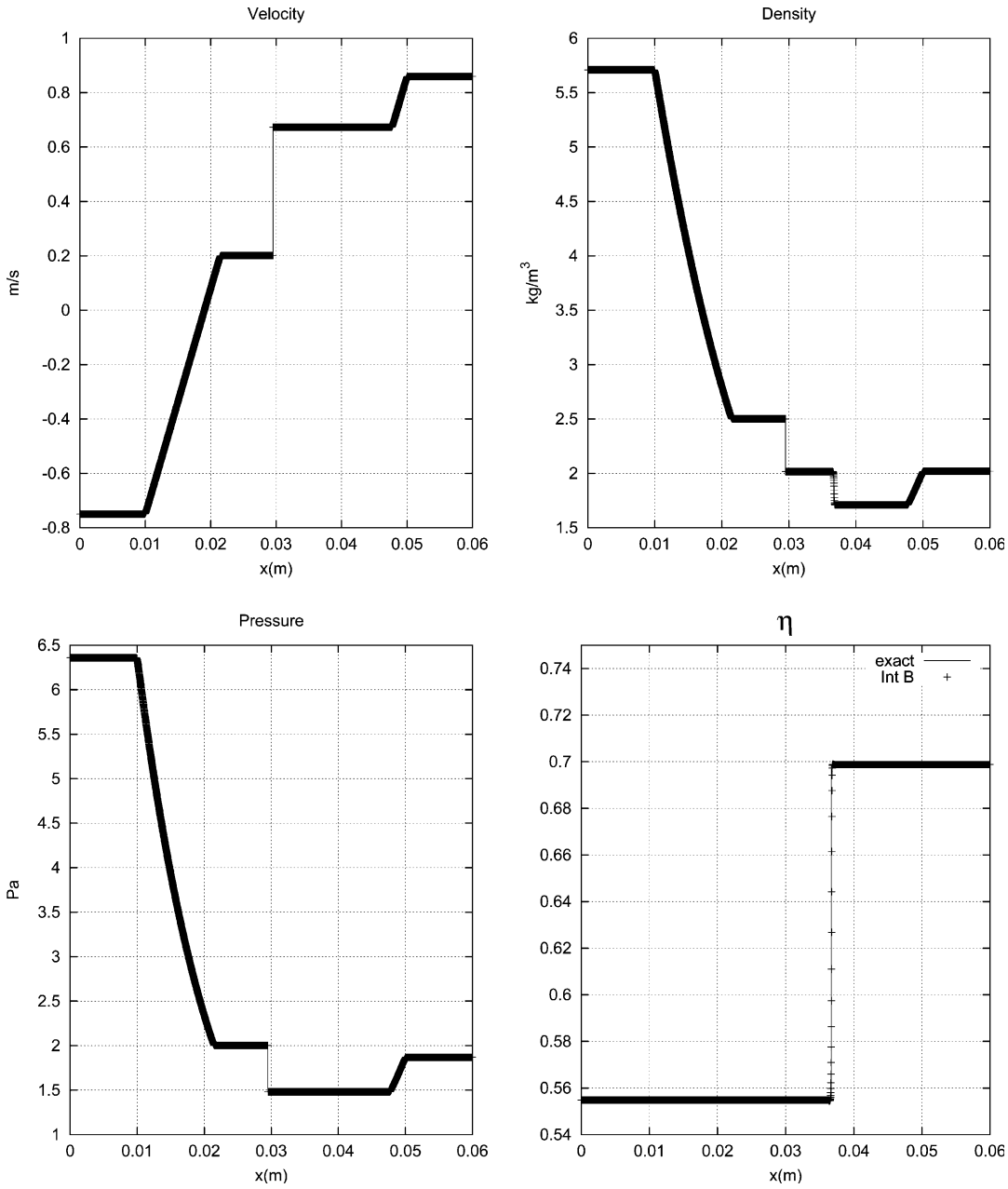

Fig. 20. Gas-phase solution at 0.01 s: internal boundary Roe on 12,000 cell mesh.

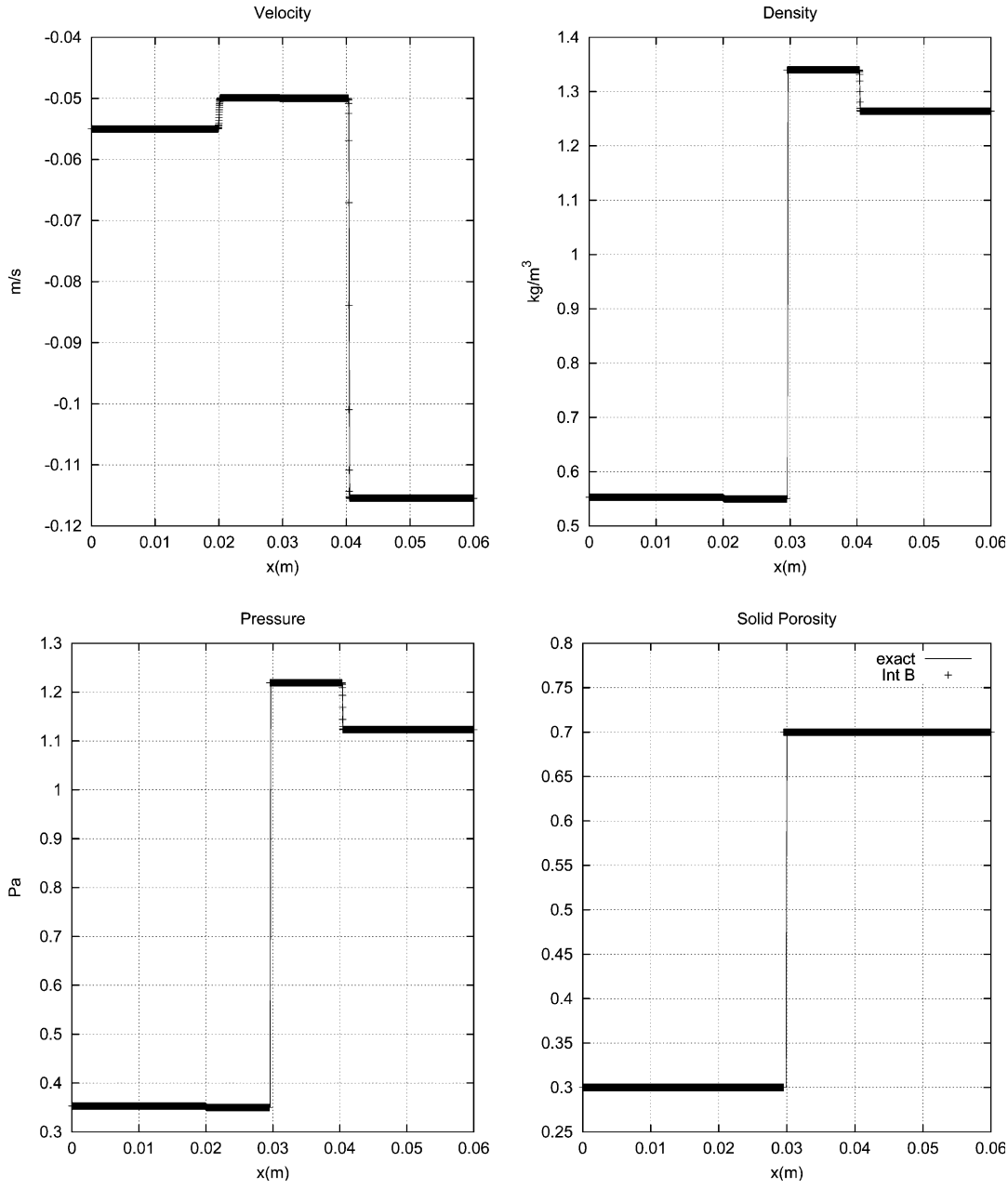

Fig. 21. Solid-phase solution at 0.01 s: internal boundary Roe on 12,000 cell mesh.

$$[u_s]_- = [u_s]_+, \tag{32}$$

$$[\eta]_- = [\eta]_+, \tag{33}$$

$$[\eta_s]_- = [\eta_s]_+, \tag{34}$$

$$\left[\phi\rho(u_s - u_g)\right]_- = \left[\phi\rho(u_s - u_g)\right]_+, \tag{35}$$

$$\left[\phi p + \phi_s p_s + \phi\rho(u_s - u_g)^2\right]_- = \left[\phi p + \phi_s p_s + \phi\rho(u_s - u_g)^2\right]_+, \tag{36}$$

$$\left[\frac{(u_s - u_g)^2}{2} + \frac{\gamma p}{\rho(\gamma - 1)}\right]_- = \left[\frac{(u_s - u_g)^2}{2} + \frac{\gamma p}{\rho(\gamma - 1)}\right]_+, \tag{37}$$

where $[\cdot]_-$ and $[\cdot]_+$ are conditions to the left and right of the compaction wave. All other waves and the behaviour of these are then identical to the normal behaviour of shocks and rarefaction for the Euler equations in the individual phases.

Note that direct comparison between the equations that describe the jump condition at the porosity interface, Eqs. (15)–(17) and the Riemann invariants in Eqs. (32)–(37) are such that the latter equations directly reduce to the former under the conditions $u_s \equiv 0$.

As in Section 5.3, we might expect any conservative numerical method that successfully maintains the jump conditions (32)–(37) to successfully capture the complete solution in all other parts of the domain that (away from the compaction wave) are fully conservative. To avoid inaccuracies related to shock-wave propagation and the nonconservative method of solution, the inverse solution will be based on rarefaction and contact waves.

6.1.1. Solid steady-state problem

The first test problem involves unsteady behaviour in the gas phase but the initial conditions for the solid phase have been specifically selected so that the solid-phase solution should remain steady. From this it can be determined whether the numerical methods are able to preserve steady-state conditions in the solid phase. Fig. 12 displays the form of the exact solution that we wish to simulate: In the gas phase, the heads ($\frac{dx}{dt} = u_R + a_R$ and $\frac{dx}{dt} = u_L - a_L$) of two expansion waves are travelling at ±2 m/s along with a contact travelling at velocity $u = 0.74$ m/s. The porosity to the left of the solid material contact – labelled region 'A' in the picture – is 0.7 and the gas pressure and density in this region are 2.0 Pa and 2.5 kg/m^3, respectively. In the solid phase, pressure and density are 0.35 Pa and 0.55 kg/m^3, respectively and $u_s \equiv 0$. Use of the jump conditions provided in Eqs. (32)–(37) along with inverse rarefaction solutions infer that the initial conditions for this problem are those detailed in Table 1.

Figs. 13 and 14 compare the conservative centred FORCE solution and nonconservative solution with the exact solution. The gas-phase profiles show reasonable agreement with the exact solutions although some discrepancy between the exact and numerical solutions is clear in the gas-phase entropy plot. As $\Delta\phi$ reduces across the interface, numerical errors will reduce – unlike the results seen in the previous section, the change in ϕ is sufficiently modest that the numerical errors are simply not visible. However, for the solid-phase profiles, seen in Fig. 14, there are visible numerical errors: The exact solution remains steady with zero velocity but both numerical solutions are unsteady, most notably characterised by regions with significant velocity gradients. Both methods do not capture the correct conditions on either side of the porosity jump; the consequence of this is that the pressure and density are locally depressed below their true values which results in the propagation of two expansion fans, both purely numerical artefacts.

Figs. 15 and 16 illustrate the solutions using the unsplit Roe-method and internal boundary method (that in this case has been applied to the conservative centred method). Note that both these methods have been *designed* to exploit information about the exact solution of the problem across the porosity jump. The discretisation for the source term $p\frac{\partial\phi}{\partial x}$ that is required for the Roe-type method is analogous to that seen in Eq. (29) where it is the entropy in the steady-state solid phase that remains constant across the compaction wave:

$$\left(\frac{p'}{\phi}\right)_I (\phi_{i+1} - \phi_i) = -\Delta(\phi_s(\rho_s u_s^2 + p_s)). \tag{38}$$

Both the Roe-type method and internal boundary method correctly capture the solution in both gas and solid phases.

The simulation has been repeated for the case in which the solid also involves a two-expansion solution travelling at ± 1 m/s and a solid contact travelling at 0.05 m/s, as illustrated in Fig. 17 (see Table 2 for details of the initial conditions). Figs. 18 and 19 compare the split-conservative centred and nonconservative numerical solutions with the exact solution. The same features are seen across the compaction wave, that is the solid velocity does not remain constant. Figs. 20 and 21 display the solutions using the internal boundary method in the Roe-solver. No solution has been produced for the Roe-solver that does not rely on the internal boundary method for this problem. At this stage no suitable discretisation of the source terms has been developed. [1]

All the numerical artefacts displayed in the above figures relate to deficiencies in the methods with respect to preserving steady-state jump conditions across the porosity jump.

Successful development of numerical techniques for this problem might involve use of the internal boundary method, which by construction, ensures that the correct jump conditions are preserved across the compaction wave. However, this method requires the exact solution of the full two-phase equations – which in general may be of prohibitive computational expensive.

The work suggests that a numerical discretisation that satisfies:

$$\mathbf{A}(\mathbf{V})\mathbf{V}_x \equiv 0$$

across cells in which ϕ does not remain constant is required to achieve the correct solution. It is possible to derive discretisations for the unsplit Roe-type method that satisfy this constraint but currently these are extracted from prior knowledge of the exact solution.

7. Conclusion

Numerical methods of solution have been employed to solve shock-tube type problems in single- and multi-phase flows. These problems involve discontinuous jumps in porosity which mean that the governing equations cannot be written in conservation form.

Exact solutions have been directly compared with solutions produced by conservative and nonconservative numerical methods. These standard techniques do not capture the correct solution. The reason is because the methods do not preserve the correct steady-state solution across jumps in porosity. The steady-state condition that holds across porosity jumps is very different from the conditions that hold across standard contact discontinuities in single-phase flows. The conditions are categorised by jumps in gas pressure, density and velocity. Gas-phase entropy, solid-phase entropy and solid-phase velocity remain constant.

If conservative numerical schemes are modified to ensure that the correct steady-state condition is maintained across porosity jumps, by exploiting the use of the exact solution across the jump, for example, then the solution is correctly resolved in all other regions. Any numerical discretisation must be designed to preserve the correct steady-state jump conditions across the porosity jump. This has been demonstrated by deriving discretisations for an unsplit Roe-type method maintaining constant gas-phase and solid-phase entropy across the porosity jump.

[1] This problem differs from the problems seen above as the compaction wave is no longer stationary.

Acknowledgements

EPSRC and DSTL jointly funded this project that is lead by Professor John Field, Cavendish Laboratory, University of Cambridge. Many thanks to Professor R.J. LeVeque (University of Washington) and Professor E.F. Toro (Trento University) for their useful suggestions. Further thanks to Dr. A. Longbottom (Fluid Gravity, St. Andrews) for providing additional feedback and computations. The reviewers did an excellent job of scrutinizing this work and have improved the overall content and readablility of the paper.

Appendix A. FORCE Algorithm

A conservative first-order centred method of solution, as presented in [15], is employed. Let $\mathbf{U}_i^n$ be some cell centred average of the vector of conserved variables in cell i at time-level n. The algorithm is two-step in which the first intermediate step is defined as

$$\mathbf{U}_{i+1/2}^{n+1/2} = \frac{1}{2}(\mathbf{U}_i^n + \mathbf{U}_{i+1}^n) - \frac{1}{2}\frac{\Delta t}{\Delta x}\left(\mathbf{F}(\mathbf{U}_{i+1}^n) - \mathbf{F}(\mathbf{U}_i^n)\right).$$

The second-step is then defined as

$$\mathbf{U}_i^{n+1} = \frac{1}{2}(\mathbf{U}_{i-1/2}^{n+1/2} + \mathbf{U}_{i+1/2}^{n+1/2}) - \frac{1}{2}\frac{\Delta t}{\Delta x}\left(\mathbf{F}(\mathbf{U}_{i+1/2}^{n+1/2}) - \mathbf{F}(\mathbf{U}_{i-1/2}^{n+1/2})\right).$$

It should be noted that second-order extensions to this method are also described in [15].

Appendix B. Operator splitting

Operator splitting enables a complex system to be split into smaller subproblems that may be solved. The method will be applied to the problem:

$$\mathbf{U}_t + \mathbf{F}_x(\mathbf{U}) = \mathbf{S}(\mathbf{U}, \phi_x). \tag{B.1}$$

Consider a numerical methodology that involves solving the system of equations given by (B.1) over time Δt. Let the solution at the initial time t be given as $\mathbf{U}^n$ so that the objective is to evolve the solution to provide $\mathbf{U}^{n+1}$ at the new time-level $t + \Delta t$. The operator splitting approach provides the following sequence of problems:

Hyperbolic system:

$$\frac{\partial \mathbf{U}}{\partial t} + \mathbf{F}(\mathbf{U})_x = 0$$

with initial conditions $\mathbf{U}^n$. The solution of this subproblem can be provided from many shock-capturing methods – in this work it is obtained using the Godunov and FORCE method. Let the solution of this be given as $\mathbf{U}'^n$.

System of ordinary differential equations: Let $\mathbf{U}'^n$ be the initial condition for the ODE:

$$\frac{\partial \mathbf{U}}{\partial t} = \mathbf{S}(\mathbf{U}, \phi_x) \tag{B.1}$$

in which the source term is discretised as

$$\left(p\frac{\partial \phi}{\partial x}\right)_i^{\prime n} \approx p_i'^n\left(\frac{\phi_{i+1}'^n - \phi_{i-1}'^n}{2\Delta x}\right).$$

The solution of Eq. (B.1) is the final evolved solution at the new time-level $\mathbf{U}^{n+1}$. ODE solvers are employed to solve this.

Appendix C. Roe-type wave propagation algorithm

The numerical method of solution described in [6] has been adopted. This method is a Roe-type method in which waves are based directly on flux differences and which can include the contribution of source terms. Consider the problem:

$$\mathbf{U}_t + \mathbf{F}_x(\mathbf{U}) = \mathbf{S}(\mathbf{U})$$

the solution of which typically consists of m waves of speed s^p where $p = 1, 2, \ldots, m$. We wish to solve the Riemann problem by performing a flux-based wave decomposition in which the flux difference plus source term contribution is written as a linear combination of the eigenvectors of the Jacobian of $\mathbf{F}(\mathbf{U})$:

$$\mathbf{F}(\mathbf{U}_i) - \mathbf{F}(\mathbf{U}_{i-1}) - \Delta x S_{i-1/2} \equiv \sum_{p-1}^{m} \beta^p_{i-1/2} r^p_{i-1/2}.$$

That is, we rewrite the left-hand side of the equation above as a linear combination of the eigenvectors $r^p_{i-1/2}$ in which the coefficients β are such that:

$$\beta^p_{i-1/2} = R^{-1}_{i-1/2}(\mathbf{F}_i(\mathbf{U}_i) - \mathbf{F}_{i-1}(\mathbf{U}_{i-1}) - \Delta x S_{i-1/2}) \tag{C.1}$$

in which R is the matrix of right eigenvectors.

The conservative update is given as

$$\mathbf{U}^{n+1}_i = \mathbf{U}^n_i - \frac{\Delta t}{\Delta x}\left(F_{i+1/2} - F_{i-1/2}\right)$$

in which:

$$F_{i+1/2} = \sum_{p:s_{i+1/2}>0} \beta^p_{i+1/2} r^p_{i+1/2},$$
$$F_{i-1/2} = \sum_{p:s_{i-1/2}<0} \beta^p_{i-1/2} r^p_{i-1/2}$$

in which $s^p_{i+1/2}$ is the pth wave-speed for Riemann problem $[i, i+1]$ and $r^p_{i+1/2}$ is the corresponding eigenvector.

As in the regular Roe method, coefficients β can then be obtained as linear combinations of the flux difference with source term contribution using Eq. (C.1). A suitable discretisation of the source contribution $S_{i-1/2}$ is required and is described in Section 5.2.

Appendix D. Nonconservative algorithm

A nonconservative first-order centred method of solution, as presented in [16], is employed. Let $\mathbf{V}^n_i$ be some cell centred average of the vector of primitive variables in cell i at time-level n. The algorithm is two-step in which the first intermediate step is defined as

$$\mathbf{V}^{n+1/2}_{i+1/2} = \frac{1}{2}(\mathbf{V}^n_i + \mathbf{V}^n_{i+1}) - \frac{1}{2}\frac{\Delta t}{\Delta x}\hat{\mathbf{A}}_{i+1/2}(\mathbf{V}^n_{i+1} - \mathbf{V}^n_i),$$

where

$$\hat{\mathbf{A}}_{i+1/2} \equiv \mathbf{A}\left(\frac{1}{2}(\mathbf{V}_i^n + \mathbf{V}_{i+1}^n)\right).$$

The second-step is then defined as

$$\mathbf{V}_i^{n+1} = \frac{1}{2}(\mathbf{V}_{i-1/2}^{n+1/2} + \mathbf{V}_{i+1/2}^{n+1/2}) - \frac{1}{2}\frac{\Delta t}{\Delta x}\hat{\mathbf{A}}_i(\mathbf{V}_{i+1/2}^{n+1/2} - \mathbf{V}_{i-1/2}^{n+1/2}),$$

where

$$\hat{\mathbf{A}}_i \equiv \mathbf{A}\left(\frac{1}{2}(\mathbf{V}_{i-1/2}^{n+1/2} + \mathbf{V}_{i+1/2}^{n+1/2})\right).$$

It should be noted that second-order extensions to this method are also described in [16].

Appendix E. Eigenstructure of the two-phase system

The Jacobian of the flux function $F(\mathbf{U})$ of the two-phase system given in Eq. (30) is:

$$J = \begin{pmatrix} J_g & 0 & 0 \\ 0 & J_s & 0 \\ 0 & J_\phi & u_s \end{pmatrix}, \tag{E.1}$$

where

$$J_k = \begin{pmatrix} 0 & 1 & 0 \\ \frac{1}{2}(\gamma_k - 3)u_k^2 & (3-\gamma_k)u_k & \gamma_k - 1 \\ \frac{1}{2}(\gamma^k - 1)u^3 - uH^k & H^k - (\gamma_k - 1)u_k^2 & \gamma_k u_k \end{pmatrix}, \tag{E.2}$$

where $k = s$ for the solid phase.

$$J_\phi = \begin{pmatrix} \frac{-u_s}{\phi_s} & \frac{1}{\phi_s} & 0 \end{pmatrix}. \tag{E.3}$$

The eigenvalues are:

$$u_g - c_g, \quad u_g, \quad u_g + c_g, \quad u_s - c_s, \quad u_s, \quad u_s + c_s, \quad u_s \tag{E.4}$$

with right eigenvectors (columns tie with speed):

$$\begin{pmatrix} 1 & 1 & 1 & 0 & 0 & 0 & 0 \\ u_g - c_g & u_g & u_g + c_g & 0 & 0 & 0 & 0 \\ H_g - u_g c_g & 1/2u_g^2 & H_g + u_g c_g & 0 & 0 & 0 & 0 \\ 0 & 0 & 0 & 1 & 1 & 1 & 0 \\ 0 & 0 & 0 & u_s - c_s & u_s & u_s + c_s & 0 \\ 0 & 0 & 0 & H_s - u_s c_s & 1/2u_s^2 & H_s + u_s c_s & 0 \\ 0 & 0 & 0 & 1/\phi_s & 0 & 1/\phi_s & 1 \end{pmatrix}. \tag{E.5}$$

The system in Eq. (30) can also be rewritten in the following nonconservative form:

$$\mathbf{V}_t + \mathbf{A}(\mathbf{V})_x = 0,$$

where

$$\mathbf{V} = \begin{pmatrix} \rho \\ u \\ p \\ \phi_s \\ \rho_s \\ u_s \\ p_s \end{pmatrix}, \quad \mathbf{A}(\mathbf{V}) = \begin{pmatrix} u & \rho & 0 & \frac{\rho}{\phi}(u_s - u) & 0 & 0 & 0 \\ 0 & u & 1/\rho & 0 & 0 & 0 & 0 \\ 0 & \gamma p & u & \frac{\gamma p}{\phi}(u_s - u) & & & \\ 0 & 0 & 0 & u_s & 0 & 0 & 0 \\ 0 & 0 & 0 & 0 & u_s & \rho_s & 0 \\ 0 & 0 & 0 & \frac{(p_s - p)}{\rho_s \phi_s} & 0 & u_s & 1/\rho_s \\ 0 & 0 & 0 & 0 & 0 & \gamma p_s & u_s \end{pmatrix}.$$

For the problems considered above, initial conditions defined in Table 2 will be applied to a domain that is 0.06 m and the interface between the left and right states is positioned at the midpoint.

References

[1] N. Andrianov, G. Warnecke, On the solution to the Riemann problem for the compresisble flow in a duct, SIAM Journal on Applied Mathematics 64 (2004) 878–901.

[2] N. Andrianov, G. Warnecke, The Riemann problem for the Baer and Nunziato model for two-phase model, Journal of Computational Physics 195 (2) (2004) 434–464.

[3] B.W. Asay, S.F. Son, J.B. Bdzil, The role of gas permeation in convective burning, International Journal of Multiphase Flow 22 (5) (1995) 923–952.

[4] M.R. Baer, J.W. Nunziato, A two-phase mixture theory for the deflagation-to-detonation transition (DDT) in reactive granular materials, Journal of Multiphase Flow 12 (6) (1986) 861–889.

[5] M.R. Baer, J.W. Nunziato, P.F. Embid, Deflagration-to-Detonation Transition in Reactive Granular Materials, Progress in Astronautics and Aeronautics Series, vol. 66, 1979, pp. 481–512.

[6] D.S. Bale, R.J. LeVeque, S. Mitran, J.A. Rossmanith, A wave propagation method for conservation laws and balance laws with spatially-varying flux functions, SIAM Journal of Scientific Computing 24 (3) (2002) 955–978.

[7] J.B. Bdzil, S.F. Son, Engineering models of deflagration-to-detonation transition, Technical Report LA-12794-MS, UC-741, Los Alamos, Los Alamos National Laboratories, NM 87545, 1995.

[8] P.S. Gough, F.J. Zwarts, Modeling heterogenous two-phase flow, AIAA Journal 17 (1) (1979) 17–25.

[9] J.M. Greenberg, A.Y. Leroux, R. Baraille, A. Noussair, Analysis and approximation of conservative laws with source terms, SIAM Journal of Numerical Analysis 34 (5) (1997) 1980–2007.

[10] A.W. Horst, G.E. Keller, P.S. Gough, New directions in multiphase flow interior ballistic modeling, Technical Report BRL-TR-3102, Ballistics Research Laboratory, Aberdeen Proving Ground, MD, 1990.

[11] C.A. Lowe, J.F. Clarke, Aspects of solid propellant combustion, Philosophical Transactions of the Royal Society, Combustion Science Thematic Volume 357 (1764) (1999) 3639–3654.

[12] L. Sainsaulieu, Finite volume approximation of two-phase-fluid flows based on an approximate Roe-type Riemann solver, Journal of Computational Physics 121 (1994) 1–28.

[13] R. Saurel, R. Abgrall, A multiphase godunov method for compressible multifluid and multiphase flows, Journal of Computational Physics 150 (1998) 425–467.

[14] E.F. Toro, Riemann-problem based techniques for computing reactive two-phase flows, in: Dervieux, Larrouturou (Eds.), Lecture Notes in Physics, Numerical combustion, vol. 351, Springer, Berlin, 1989.

[15] E.F. Toro, Riemann Solvers and Numerical Methods for Fluid Dynamics, first ed., Springer, Heidelberg, 1997.

[16] E.F. Toro, A. Sviglia, PRICE: Primitive centred schemes for hyperbolic systems, International Journal for Numerical Methods in Fluids 42 (2003) 1263–1291.